TUTORIAL REVIEW

From lignin to jet fuel: advancing selective cyclohydrocarbon production toward full compatibility with aviation standards

Jianyu Wang, [a,b,c] Zheng Li, [c] Chun Zhao, ID *[a] Jing Zhang, ID *[a] Aiguo Wang, [c] Liquan Jing, ID [c] Na Zhong, [c] Zhangxin Chen[c] and Jinguang Hu ID *[c]

Sustainable aviation fuel (SAF) derived from lignocellulosic biomass represents a critical pathway to decarbonizing the aviation sector. As the only abundant, naturally aromatic biopolymer, lignin offers unique potential for producing cyclic hydrocarbons compatible with conventional jet fuels. This review critically examines recent advances in lignin valorization strategies, focusing on two key stages: (i) the depolymerization of lignin into phenolic-rich bio-oils, and (ii) the selective hydrodeoxygenation (HDO) of these intermediates into cycloalkanes and arenes. Emphasis is placed on catalytic design, reaction engineering, and solvent systems that improve product selectivity and mitigate harsh HDO conditions. The conversion of lignin typically begins with the production of bio-oil containing phenolic monomers and dimers, which is then followed by HDO to convert these precursors into cycloalkanes primarily. This review examines and compares various methods for producing lignin bio-oil for jet fuel applications. It then explores strategies to improve the selectivity of cycloalkanes or arenes during the HDO process, highlighting effective approaches to mitigate the challenging reaction conditions associated with HDO. The review further analyzes the structural and physicochemical differences between lignin-derived hydrocarbons and certified jet fuels, underscoring the remaining challenges in achieving full compatibility, such as energy density, volatility, and combustion properties. In addition, this review assesses the environmental impacts and economic viability of producing cycloalkane-rich SAFs from lignin. Despite significant progress, the synthesis of a 100% lignin-based SAF blend remains unachieved, highlighting the need for an integrated framework that couples molecular-level fuel design with comprehensive performance metrics. This roadmap is essential to guide future research and industrial-scale implementation of lignin-based SAF.

Green foundation

1. This review highlights recent advances in catalytic lignin valorization into cyclic hydrocarbons for sustainable aviation fuels (SAFs), emphasizing green chemistry principles such as renewable feedstocks, selective and energy-efficient catalysis, and replacement of fossil-derived hydrogen and solvents.

2. Converting lignin into jet fuels addresses two global challenges: aviation decarbonization and biomass waste valorization. As the most abundant renewable aromatic biopolymer, lignin enables renewable, drop-in fuels compatible with existing infrastructure, offering both industrial and environmental benefits.

3. The future hinges on bridging molecular and performance gaps between lignin-derived hydrocarbons and conventional jet fuels. Fully lignin-based fuels lack ASTM approval; this review outlines green strategies—*in situ* hydrogen generation, mild oxygen removal, and fuel pre-screening—that advance 100% renewable, drop-in SAFs.

1. Introduction

Decarbonizing aviation is a critical challenge, and sustainable aviation fuel (SAF) derived from biomass has emerged as a promising solution.[1] Unlike renewable electricity, biofuels offer the advantage of carbon sequestration during feedstock growth: the CO_2 released when SAF is burned is partially offset by the CO_2 absorbed during photosynthesis. Lifecycle analyses indicate that SAF can cut greenhouse gas emissions (GHG) by roughly 50% up to >90% compared to fossil jet fuel, depend-

[a]College of Environment and Ecology, Chongqing University, Chongqing 400044, China. E-mail: pureson@cqu.edu.cn, zhangjing2018@cqu.edu.cn
[b]Forest Products Biotechnology/Bioenergy Group, University of British Columbia, Vancouver, BC, V6T 1Z4, Canada
[c]Department of Chemical and Petroleum Engineering, University of Calgary, 2500 University Drive, NW, Calgary, AB T2N1N4, Canada. E-mail: jinguang.hu@ucalgary.ca

ing on feedstock and production pathway.[2–4] International Energy Agency (IEA) projects that bio-jet fuel could reach about 3.5% of global aviation demand by 2028 under accelerated adoption scenarios, reflecting growing interest in scaling SAF production.

Currently, all commercially used SAF/bio-jet fuel is produced from oleochemical feedstocks, such as fats, oils, greases (FOGs), or vegetable oils (*e.g.* soybean, canola) *via* the hydroprocessed esters and fatty acid (HEFA) pathway. HEFA-SAF is already approved by the American Society for Testing and Materials (ASTM) for blending up to 50% with conventional jet fuel.[5–7] However, relying on edible oils for fuel poses sustainability and scalability concerns. It creates competition with food supply and offers only moderate carbon reductions once indirect emissions (from fertilizer use, diesel farming equipment, land-use change, *etc.*) are accounted for.[8,9] Indeed, life cycle emission reductions for HEFA SAF are often in the range of only ~50–65% *versus* petroleum jet.[10] There are also practical limits to waste-oil availability. In the U.S., non-food lipid feedstock could support at most about 1.7 billion gallons per year of HEFA fuel–insufficient for long-term demand.[11] Therefore, more sustainable and abundant feedstocks such as lignocellulosic biomass (agricultural residues, forestry byproducts, energy crops) are being explored to supplement or replace lipid-based feedstocks.[12–14]

Lignin, a major component of lignocellulose, is a particularly attractive feedstock for SAF. Lignin is a three-dimensional aromatic polymer comprising *p*-hydroxyphenyl (H), guaiacol (G), and syringyl (S) phenolic units linked by ether and C–C bonds.[15–17] It is the second most abundant natural polymer in wood (making up ~15–40% of dry wood) and the largest renewable reservoir of aromatic rings on Earth.[18] Huge quantities of lignin are generated as a low-value byproduct in the pulp & paper and bioethanol industries (on the order of 50–70 million tons annually worldwide), yet over 98% of it is simply burned for process heat rather than upgraded into products.[19,20] This underutilized aromatic resource could be redirected as feedstock for jet fuel production. Lignin chemical structure (rich in aromatic rings) is well suited for producing the cyclic hydrocarbons (both aromatics and cycloalkanes) that are essential components of jet fuel.[21] In contrast to fatty-acid-based fuels that yield mostly linear alkanes in the diesel range, lignin can directly generate monocyclic, bicyclic, and tricyclic hydrocarbon molecules in the jet fuel boiling range with minimal additional carbon-chain building. This gives confidence in lignin's potential as a feedstock to produce "drop-in" jet fuel blendstocks with the required cyclic structures.[21,22]

Cyclic hydrocarbons are indispensable components of traditional jet fuel, with cycloalkanes and aromatics comprising 32.9% and 21.2% of commercial aviation fuel Jet-A, respectively. Conventional jet fuel contains 8–25% v/v aromatic compounds to ensure O-ring swelling capabilities, preventing fuel leakages.[23] Cycloalkanes have lower H/C ratios, higher densities, and lower heat release per unit mass than *n*/iso-alkanes, while exhibiting higher H/C ratios and lower densities than

aromatic compounds.[24] Lignin-derived, cycloalkane-rich hydrocarbons, which inherently comprise a mixture of *in situ*-generated mono- and dicyclic cycloalkanes alongside a small fraction of n/iso-alkanes, show strong potential as fully synthetic jet fuels (FSJF). This composition directly results in a superior property profile, including enhanced density, volumetric energy content, low-temperature fluidity, and reduced soot emissions, while preserving the necessary O-ring swelling capability, as detailed in Section 4.[21,25,26] Currently, both one-step and two-step catalytic conversion pathways have garnered significant attention. However, the two-step approach is favored for FSJF synthesis, as it not only minimizes the risk of catalyst deactivation but also alleviates the severity of conditions typically associated with the HDO process.[22] Compared to oleochemical feedstocks, lignin-derived hydrocarbons fall more naturally within the jet fuel range, while those from vegetable oils are generally closer to the diesel range.[27] The catalytic conversion process for lignin is more straightforward than that for oleochemical feedstocks, which require additional steps such as hydrocracking, isomerization, and cyclization, alongside HDO.[22,25,28,29] Lignin, therefore, represents a promising feedstock for directly producing alkanes with desirable cyclic and isomeric structures that meet the chemical criteria for jet fuel applications.[3]

Despite the promise of lignin as a feedstock for SAF, the path from lignin to jet fuel remains a complex challenge. While numerous studies have focused on individual steps of lignin conversion, such as lignin-derived oil extraction,[30–32] oil upgrading,[23,33–35] and sustainability and technoeconomic assessments,[36] comprehensive reviews addressing the full lignin-to-jet-fuel pathway are limited.[16] Each step in this process must be carefully optimized, as catalyst types and reaction conditions vary significantly depending on whether the goal is SAF production or high-value chemical synthesis.

This review seeks to address this gap by presenting a comprehensive overview of current lignin conversion pathways and catalytic technologies for SAF production. Particular attention is given to the properties of lignin-derived oils produced *via* lignin-first biorefining or depolymerization of isolated lignin. These properties, determined by feedstock, conversion configuration, and catalyst selection, greatly influence the severity of subsequent HDO and the chemical structure of the final hydrocarbon products. The review begins by comparing pathways for producing lignin bio-oils and identifying optimal catalytic configurations for their extraction. It then focuses on advanced HDO strategies tailored to the specific requirements of SAF applications. As summarized in Fig. 1, upgrading lignin typically requires more hydrogen than oleochemical feedstocks, necessitating the use of high-intensity hydrogen during the valorization processes.[5] To address this, the review emphasizes conversion strategies that minimize fossil energy input and operate under milder conditions. Finally, it is important to note that lignin-derived jet fuels have not yet received ASTM certification, highlighting the need for continued research and comprehensive evaluation of recent advancements in this area.
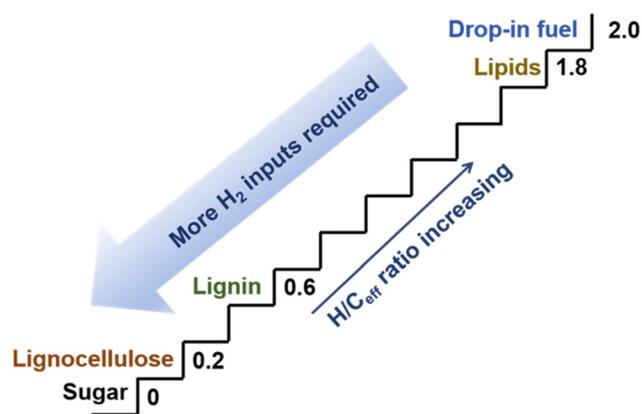
Fig. 1 The effective hydrogen-to-carbon ratio 'staircase' for different feedstocks, reproduced from ref. 5 with permission from John Wiley & Sons, copyright 2019.

2. Bio-oil from lignin for jet fuel production

2.1 Extracting lignin-derived oil from lignocellulose

The majority of commercially produced lignin today is a by-product of the pulp and paper industry, where the primary aim is to remove lignin to obtain cellulosic materials used for paper, packaging, or as chemical feedstocks for products such as cellulose acetates and nitrates.[37] The harsh pulping conditions promote the formation of stable C–C bonds, making lignin more recalcitrant and limiting the yield of monomers and low-molecular-weight oligomers.[38,39] To address this, the "lignin-first" strategy has been proposed, focusing on obtaining a more reactive form of lignin. This biorefinery strategy seeks to maximize the value of biomass's lignin and polysaccharide components by selectively depolymerizing lignin while preserving and utilizing the cellulose and hemicellulose fractions.[39,40]

2.1.1 Reductive catalytic fractionation (RCF) of lignocellulose. Reductive catalytic fractionation (RCF) is a promising lignin-first strategy that enables the extraction of native lignin from biomass while preserving β-O-4 linkages and simultaneously depolymerizing it into bio-oil enriched with functionalized phenolic monomers and dimers.[41] The extent of lignin depolymerization and the composition of the resulting bio-oil are significantly influenced by process parameters such as biomass feedstock, reaction temperature, solvent composition, and catalyst type.[36,42] Heterogeneous bifunctional catalysts, such as Pd/C, Pd/CN$_x$, Ni/C, and Ru/Al$_2$O$_3$, are particularly effective in cleaving β-O-4 linkages and selectively hydrolyzing carbon–hydroxyl bonds, thereby facilitating the formation of low-molecular-weight phenolics.[41,43] Additionally, a reductive environment prevents the repolymerization of unstable intermediates by hydrogenating reactive C=C side chains.[44] This not only stabilizes the lignin-derived bio-oil but also ensures a high overall oil yield (~90 wt%) in a single step, with significant monomer and dimer content.[45,46] The size of the metal particles in bifunctional metal catalysts significantly influences the selectivity for aliphatic –OH groups on monomers.[47] Metal nanoclusters and single atoms are effective in removing residual aliphatic hydroxyl groups from monomers, thereby improving the stability of lignin-derived bio-oil.[47]

The theoretical maximum lignin monomer yield is roughly proportional to the square of the relative content of cleavable inter-unit ether bonds, with C–C bonds typically remaining unbroken during RCF. A linear correlation has been established between the β-O-4 content in lignocellulose and the theoretical maximum monomer yield.[48] Feedstock origin plays a pivotal role in product distribution, as hardwood substrates preferentially generate the formation of propyl-substituted syringol (Pr-S), along with some guaiacol (Pr-G), whereas softwood substrates mainly yield Pr-G.[49] In contrast, grasses primarily produce monomers derived from *p*-coumaric and ferulic acid units. Moreover, hardwoods tend to generate more dimers than softwoods and grasses, with grasses yielding the least.[50,51] A high oligomer yield, typically associated with a low monomer yield in RCF products, is characterized by oligomers with relatively low molecular weight (M_w) and a high content of hydroxyl groups.[49]

Polar protic organic solvents are commonly employed to dissolve lignin under reductive subcritical conditions.[52] The yields of monomers and dimers, as well as the delignification efficiency, exhibit a linear relationship with solvent polarity, as quantified by the Reichardt polarity parameter (E_T^N).[42,53] Highly polar solvents exhibit superior penetration into the lignocellulosic matrix, thereby enhancing delignification and non-catalytic extraction.[42] Arts *et al.* partially recycled lignin-derived oil with methanol to maintain a high monomer yield by using a mixed solvent containing methanol, methyl acetate, water, acetic acid, and crude lignin oil, also promoting hemicellulose co-extraction.[36] They used extended reaction times, elevated temperatures, and increased hydrogen pressure to further enhance monomer yield and selectivity.[36,42] However, excessively high polarity can lead to considerable carbohydrate loss due to solubilization. To address this, lignin-first delignification efficiency (LFDE) was introduced to optimize process efficiency, ranking solvents based on their delignification and carbohydrate retention capabilities. Methanol and ethylene glycol were identified as high-performing solvents, yielding approximately 50 wt% monomers and 12 wt% dimers under optimized conditions.[53] Additionally, acidic conditions are more favorable for the production of monomers and dimers, as well as for sugar retention, compared to basic conditions.[54]

Fig. 2 illustrates the typical chemical composition of RCF oil derived from pine refinement, as reported by Thi *et al.*[55] The dominant monomer was 4-propanol guaiacol, with a yield of 34.03 wt% of monomers. Dimers (15.79 wt%) and trimeric oligomers (7.26 wt%) primarily consist of various G units connected through C–C interunit linkages, including β-5, β-1, β–β, and 5–5. Only trace amounts of β-O-4 and 4-O-5 linkages were observed in these RCF lignin oils.[55] The presence of trimers results in a distribution of excessively long carbon chains in
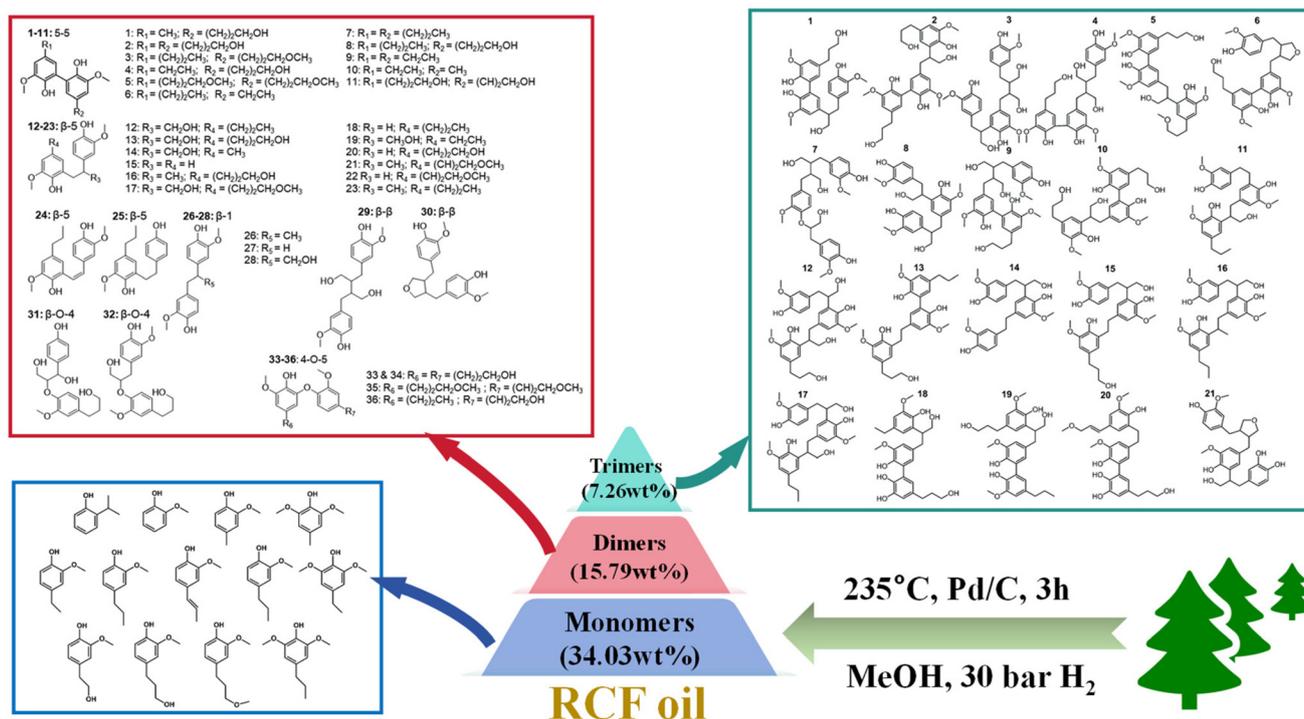
Fig. 2 The composition of monomers, dimers, and trimers in the RCF oil, along with their corresponding main chemical formulations, adapted from ref. 55 with permission from the Royal Society of Chemistry, copyright 2022.

crude oil; however, partial removal of trimers can be achieved through washing with non-polar solvents.[55]

2.1.2 Hydrogen-free and self-supplied reductive pathways. RCF typically requires high-pressure H_2 and high temperatures (above 200 °C), challenging its scale-up.[56] Due to the significant capital costs for handling organic solvents (*e.g.*, methanol) and H_2 gas, a hydrogen-free RCF approach could potentially reduce costs by 24%.[57] Deep Eutectic Solvents (DES) have been shown to delignify biomass without additional hydrogen.[58,59] Although ethylene glycol can act as a hydrogen source following depolymerization of lignin over Ru/C, as highlighted by Li *et al.*, the high proportion of choline chloride to ethylene glycol has been shown to limit the hydrogen-donating ability of ethylene glycol because of excessively strong hydrogen bond acceptor-donor interactions between choline chloride and ethylene glycol.[48] Moreover, scaling up DES-based systems remains challenging due to a limited understanding of their fundamental reaction mechanisms.[60]

Other studies have demonstrated that certain biomass substrates can produce *in situ* H_2 through hydrogenolysis and aqueous-phase reforming, thereby eliminating the need for external hydrogen sources.[61] This procedure is commonly referred to as the self-hydrogen-supplied catalytic fractionation (SCF) process. Zhou *et al.* successfully fractionated birch sawdust in an aqueous solution over a Pt/NiAl$_2$O$_4$ catalyst without the addition of a hydrogen source (Fig. 3a).[62] After a 24 hour reaction at 140 °C, the phenolic monomer yield reached 46.6 wt%, with propyl(ethyl) end-chained guaiacol

and syringol as the main products. Additionally, 90% of the cellulose was retained in the pulp. As shown in Fig. 3b, hemicellulose served as the primary hydrogen source, undergoing hydrolysis to xylose, dehydrogenation, and cleavage processes to generate CO intermediates. The water–gas shift reaction (WGS) over the Pt/NiAl$_2$O$_4$ catalyst then produced H_2 and CO_2. Li *et al.* provided insights into the catalytic conversion mechanism over Pt/NiAl$_2$O$_4$, unveiling that the presence of oxygen vacancies (O_V) on NiAl$_2$O$_4$ facilitated the reduction of PtO$_x$ to metallic Pt.[63] This promoted methanol dehydrogenation and enabled the subsequent WGS through a redox mechanism (Fig. 3c). Notably, this mechanism differed from the conventional γ-Al$_2$O$_3$ support, where the WGS proceeded *via* an associative mechanism (Fig. 3c).[63]

2.1.3 Oxidative catalytic fractionation (OCF) of lignocellulose. Oxidative catalytic fractionation (OCF) of biomass to produce lignin has been less investigated, despite certain advantages such as the use of mild reaction conditions (60–180 °C and 0.2–0.3 MPa O_2, *vs.* 160–450 °C and 1–10 MPa H_2), plus the use of "green" solvents (H_2O *vs.* organic) and cheap reagents.[64] Generally, OCF catalytic systems are still in the early stages of development. The OCF process with alkali typically initiates by cleaving ether bonds in lignin and activating C_α–C_β to form C_α=C_β through dehydration.[65] To become less reliant on alkali, a better catalyst will be required.[65,66] In more recent work, a two-step approach was used to enhance monomer yield during the OCF of wood sawdust.[67] Luo *et al.*[68] fractionated poplar biomass over a heterogeneous Co–N–C
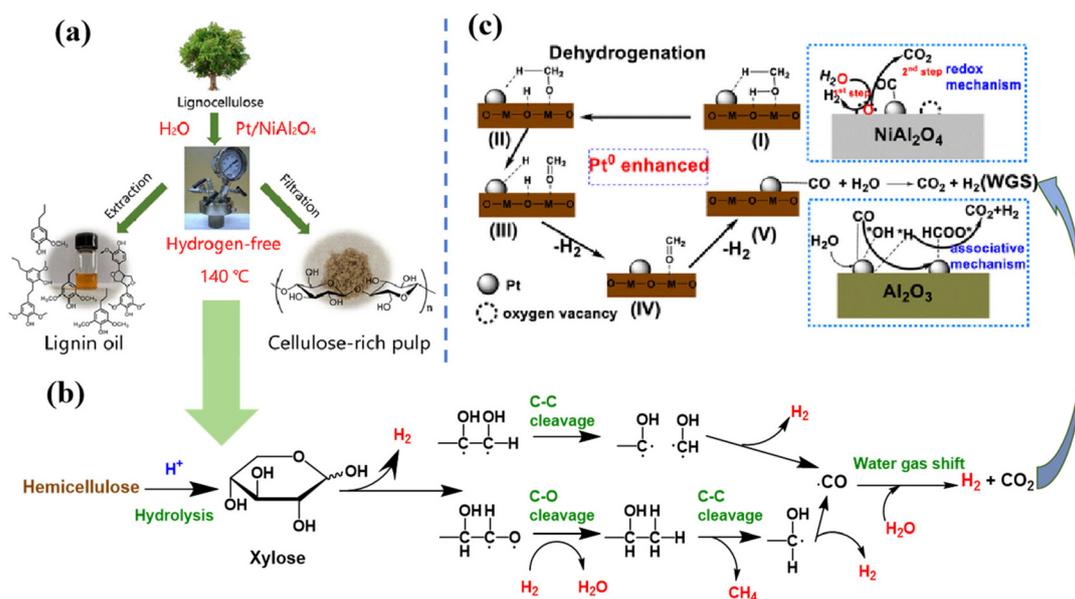
Fig. 3 (a) Production of lignocellulose-derived hydrogen *via* catalytic fractionation (SCF), reproduced from ref. 62 with permission from the American Chemical Society, copyright 2023. (b) Hemicellulose serves as a hydrogen source under hydrothermal conditions during SCF, adapted from ref. 62 with permission from the American Chemical Society, copyright 2023. (c) Catalytic mechanism for *in situ* hydrogen production over Pt/NiAl$_2$O$_4$ and Pt/γ-Al$_2$O$_3$, reproduced from ref. 63 with permission from the American Chemical Society, copyright 2019.

catalyst in non-alkaline organic solution (acetone) under 190 °C and 35 bar air atmosphere (6% O$_2$ in N$_2$). This process yielded 15 wt% of phenolic products comprising aldehydes (vanillin and syringaldehyde) and carboxylic acids (*p*-hydroxybenzoic acid, vanillic acid, and syringic acid), along with 56 wt% yields of dimers, trimers, and oligomers in the liquid stream.

Lignin-first biorefining provides notable advantages for producing high-quality lignin bio-oils, particularly by generating monomeric and dimeric precursors suitable for jet fuel synthesis, enabling complete lignocellulosic valorization, and accommodating flexible, renewable hydrogen sources. Despite substantial progress in developing RCF strategies, most RCF processes remain confined to the laboratory scale due to challenges related to hydrogen gas supply and handling of organic solvents, although recent studies indicate the potential for significant cost and carbon footprint reductions.[36] While OCF offers greener reaction conditions compared to reductive approaches, its limited monomer yield and the prevalence of over-oxidized products could introduce complexities in downstream deoxygenation processes.

2.2 Extracting lignin-derived oil from isolated lignin

The most isolated lignin from technical lignin is obtained through sulfur and sulfur-free processes based on commercial pulping technologies, such as Kraft, Sulfite, Soda, and Organosolv.[69,70] The lignoboost and lignoforce processes precipitate black liquor derived from the Kraft process, with refineries such as West Fraser Timber producing about 10 500 tons of technical lignin annually.[71] The lignosulphonates derived and marketed by companies such as Borregaard are

more reactive but already sell for a higher price and are unlikely to be used as a biofuel feedstock.[72]

Nonetheless, the widespread availability of industrial lignin has prompted researchers to explore its potential as a feedstock for various applications. As suggested by Rinaldi *et al.*,[70] eqn (1) can estimate the maximum yield of a monomer. Assessing the possibility of using lignin as a feedstock is beneficial.

$$Y = \frac{(n-2)P^2 + 2P}{n} \times 100 \qquad (1)$$

The parameter Y denotes the cumulative yield of individual monoaromatic compounds, while n represents the number of monomers present within the polymeric chain. P refers to the fraction of cleavable bonds.[70]

Fig. 4a demonstrates a positive correlation between the P-value and monomer yield. However, most downstream technical lignins (P-values below 0.2) are unsuitable as feedstock for fuel production. Genetically engineered lignins, on the other hand, show significant promise for high monomer yields. Yet, for jet fuel, focusing solely on monomers is insufficient, as a lack of dimers may prevent the final product from meeting the required length of the carbon chain. According to Phongpreecha *et al.*,[73] with a 50% β-O-4 content, the cleavage of all β-O-4 linkages yields approximately 10% tetramers, 17% trimers, 25% dimers, 27% monomers, and 21% other oligomers. Fig. 4b further highlights the disadvantages of downstream technical lignin compared to native lignin. While hardwoods excel in monomer yield, they also theoretically produce higher yields of both dimers and trimers. Although technical lignin is theoretically unsuitable as a jet fuel feedstock, its
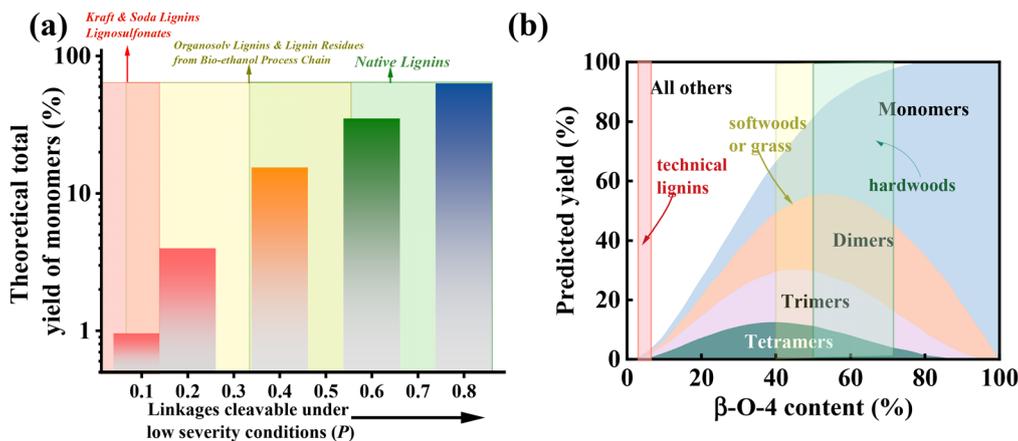
Fig. 4 (a) Graph illustrating eqn (1) for various P values, adapted from ref. 70 with permission from John Wiley and Sons, copyright 2016. (b) Predicted yield distributions for monomers, dimers, and oligomers from the cleavage of β-O-4 in a population model of lignin polymers of $n = 100$ over a range of β-O-4 contents. Figure adapted from ref. 73 with permission from the Royal Society of Chemistry, copyright 2017; data sourced from ref. 74 and 75.

availability has led many researchers to investigate it as a subject of study. Generally, in such cases, it is not sufficient to only consider C–O–C bond cleavage; the cleavage of the Csp^2–Csp^3 bond must also be taken into account.

2.2.1 Lignin oil derived *via* pyrolysis. Lignin pyrolysis generally proceeds through three stages: dehydration (<120 °C), active pyrolysis (200–450 °C), and passive pyrolysis (>450 °C) (Fig. 5).[76] During the active pyrolysis stage, thermal energy
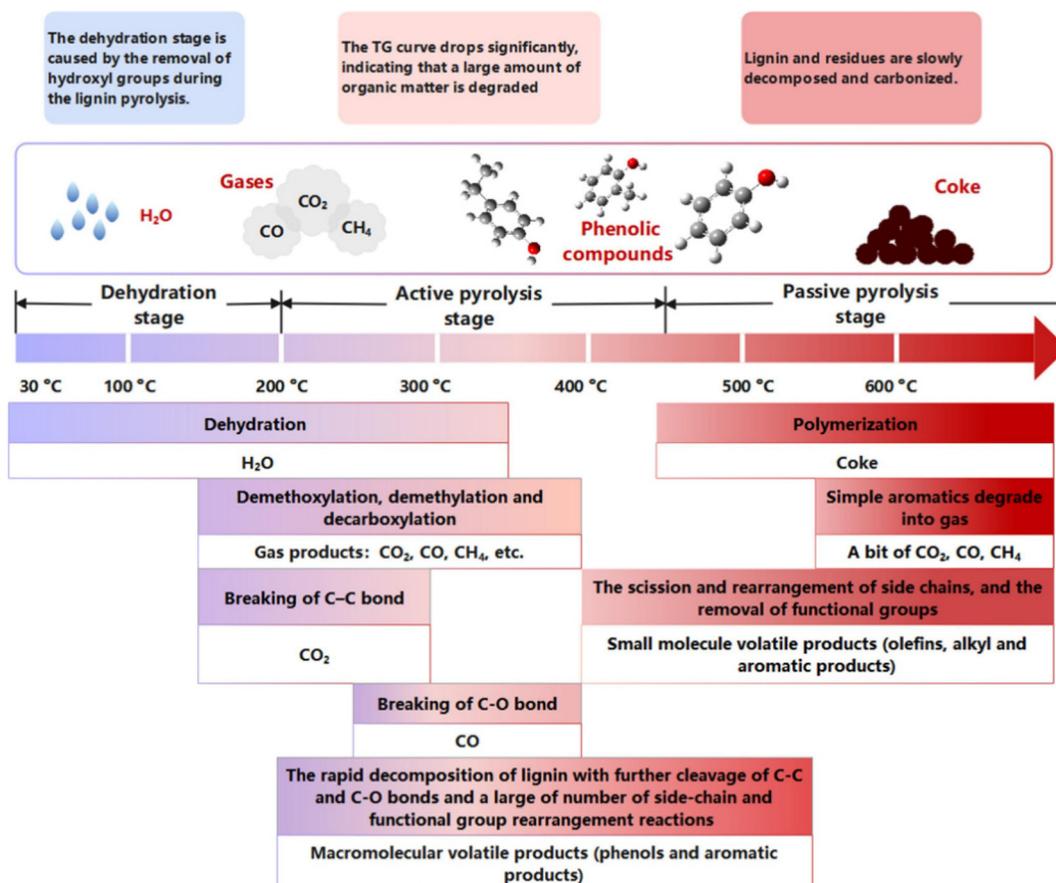

Fig. 5 Schematic summary of the lignin pyrolysis process, reproduced from ref. 76 with permission from Elsevier, copyright 2022.

breaks down interunit linkages within lignin, resulting in the formation of oxygen-containing monomers, dimers, and oligomers. The type of lignocellulosic feedstock plays a crucial role in product distribution. For instance, lignin derived from corn stover (a representative herbaceous biomass) yielded the highest phenolic monomer content (16.26% C based on lignin), followed by red oak (hardwood, 8.61% C) and loblolly pine (softwood, 9.51% C), highlighting the structural influence of different lignin sources on pyrolysis efficiency and selectivity.[77] Lower temperatures favor dimer formation, while higher temperatures increase the production of monomers and oligomers.[78] Above 525 °C, oligomers undergo secondary cracking into dimers, while temperatures above 550 °C promote the formation of fused aromatics and polycyclic hydrocarbons from phenols.[78,79]

The complexities of lignin pyrolysis mechanisms stem from its intricate structure.[80,81] Typically, the cleavage of β-O-4 linkages is driven by unimolecular decomposition, hydrogen radical abstraction, hydrogen bond-induced homolysis, or the pyrolysis-products-assisted hydrogen transfer (AHT) mechanism.[80] The concerted pericyclic cleavage is considered to be dominant for β-O-4 linkages compared to homolytic cleavage.[82] The cleavage of interunit β-1 and β-5 linkages primarily occurs through C_α–O and C_α–C_β homolytic reaction.[76] The cleavage of the 5–5′ linkage, characterized by high bond dissociation energy (BDE), typically initiates with demethylation, followed by the dehydrogenation of the edge groups.[83,84] During the passive pyrolysis stage, propanoid side-chains and oxygen-containing functional groups undergo degradation and transformation, resulting in simpler aromatic volatiles and a few gas products (e.g., CO_2, CO, H_2, and CH_4) or undergo polymerization and settle to form coke.[76]

Under optimized fast pyrolysis conditions, lignin can yield approximately 45 wt% liquid, 35 wt% char, and 16 wt% gas, with phenols and dimers reaching up to 52% and 42% in the liquid fraction, respectively.[78] The abundance of oxygen-containing functional groups in lignin holds the potential to influence the pyrolysis rate, reactivity, and distribution of pyrolysis products.[76,85,86] Phenolic hydroxyl groups emerge as the predominant functional groups, acting as electron-donating groups that diminish the stability of lignin and promote the repolymerization reaction of lignin fragments, ultimately leading to charring.[76] Consequently, several studies have emerged that aim to pretreat lignin to alleviate the adverse effects of phenolic hydroxyl groups on pyrolysis. Li et al.[87] pretreated softwood kraft lignin (SKL) by masking phenolic hydroxyl groups with propylene oxide before pyrolysis. The study revealed high selectivity (~94%) toward the oxypropylation of phenolic hydroxyl groups, thereby enhancing the hydrogen-to-carbon ratio of SKL and increasing the relative content of low-oxygen aromatic compounds. More importantly, on a lignin basis, the yield of pyrolysis oil increased from 37.1% to 44.3%, while the char yield decreased from 47.2% to 36.9% after masking the phenolic hydroxyl groups.[87] Methoxy stands out as another prevalent oxygen-containing functional group within the lignin structure, and its specific location has a discernible impact on the pyrolysis mechanism.[76,88] The presence of the methoxy group can lower the BDE of the C–O bond, thereby increasing the reactivity of the C–O hemolytic reaction.[76] However, research on other oxygen-containing functional groups is relatively limited.[81]

Catalytic fast pyrolysis, a commonly used method for converting lignin into bio-oil, can be classified into in situ and ex situ.[89] Compared to non-catalytic pyrolysis, catalyst-assisted pyrolysis can lower the decomposition temperature, accelerate the reaction rate, and improve the selectivity for oxygen-free monoaromatic hydrocarbons in the pyrolysis oil. At the laboratory level, ex situ catalytic fast pyrolysis is typically conducted using a simplified configuration in which the biomass and catalyst are arranged in separate layers within the same fixed-bed reactor.[90] In contrast, practical-scale ex situ catalytic fast pyrolysis employs two physically separated reactors: one dedicated to biomass pyrolysis and the other to catalytic vapor upgrading, enabling continuous operation. The resulting pyrolysis vapors are subsequently condensed into liquid products that spontaneously separate into an aqueous and an organic phase.[91] The cost of in situ catalytic pyrolysis mainly arises from catalyst deactivation and continuous regeneration.[91] Conversely, the considerable cost for the ex situ configuration stems from the capital investment for the two separate reactor systems. Based on an economic analysis, Li et al.[92] found that the minimum fuel selling prices (MFSPs) of the in situ and ex situ configurations were comparable. This quantitative comparison suggests that the higher operating cost resulting from catalyst replacement in the in situ process is offset by the greater capital investment required for the ex situ configuration. Catalysts for pyrolysis include inorganic salts (e.g., alkali metals), metal oxides (e.g., Al_2O_3, CaO, Fe_2O_3, and ZnO), zeolites, and biochar.[93] ZSM-5 zeolite is well-known for its highly active conversion of lignin pyrolysis intermediates and increased yield of aromatic hydrocarbons due to strong Brønsted acidity, a unique porous structure with tubular micropores of moderate size (~5.5 Å diameter), and wider spherical intersections (~10 Å diameter).[94] Additionally, zeolites are remarkably tunable for pyrolysis. Pan et al.[95] noted that zeolites with a low Si/Al ratio are beneficial for enhancing the selectivity of monocyclic aromatics in guaiacol pyrolysis, attributed to the bidentate coordination of hydroxyl groups in the guaiacol intermediate (catechol) with acidic sites of high intensity.

In summary, lignin pyrolysis is promising for producing bio-oil rich in monomers and dimers. At temperatures above 550 °C, fused dimers can also be obtained. Future research should prioritize understanding the roles of specific oxygenated groups, particularly phenolic and methoxy functionalities, in char formation and reactivity, to optimize yield and minimize coke formation.

2.2.2 Lignin oil derived via liquefaction

2.2.2.1 Hydrothermal liquefaction (HTL) of isolated lignin. Hydrothermal liquefaction (HTL) has been extensively investigated in both batch and continuous configurations. While batch systems are predominantly employed at the laboratory

scale for mechanistic and parameter optimization studies, practical-scale HTL processes are typically designed for continuous operation to ensure process stability and scalability.[96,97] HTL is a thermochemical depolymerization technique conducted in aqueous media at elevated temperatures (200–400 °C) and pressures (100–350 bar), typically without the need for external hydrogen input.[98] It facilitates the cleavage of C–C and C–O–C bonds through hydrolysis, alkylation, demethoxylation, and condensation reactions, generating phenolic-rich biocrude, biochar, water-soluble compounds, and light gases such as CO_2, CO, and CH_4.[99,100] During the HTL process, water acts as both a solvent and catalyst, providing access to ionic reaction conditions and reducing the hydrophobic properties of biomass. The HTL process is more attractive under subcritical (250–350 °C) or supercritical conditions (390–450 °C), where the dielectric constant (ε) of water declines and the ionic product (pK_w) increases considerably.[101] This will release more H_3O^+ and OH^- ions, promoting hydrolysis or elimination of interunit linkages in lignin and producing phenolics and alkyl-phenolics.[102,103] The deprotonation of hydroxyl groups in phenolics and other aromatic subunits of lignin alters the electronic structure, enhancing the solubility of lignin in water, destabilizing linkages, and facilitating bond cleavage and depolymerization, even at neutral subcritical hydrothermal conditions, which are dominated by ionic chemistry.[104,105] However, compared to subcritical conditions, supercritical conditions are likely to result in a substantial increase in char and gaseous product formation, despite the potential for a higher degree of depolymerization.[103,106]

HTL can operate in batch or continuous flow reactors, with the latter requiring careful consideration of lignin solubility to prevent solid deposition and blockage under high pressure.[107,108] The catalysts for HTL of lignin include homogeneous basic/acidic catalysts, heterogeneous alkaline earth metals, transition metals, and zeolites.[109] Zeolites typically facilitate the cleavage of the C–C bond, while transition metal catalysts enable *in situ* hydrogen production, the removal of heteroatoms, and an increase in the H/C elemental ratio of bio-oils.[109] Certain zeolites (*e.g.*, HY) exhibit increased depolymerization efficacy for condensed lignin and highly selective cleavage of the Csp^2–Csp^3 bond under HTL conditions.[110] Kong *et al.*[111] screened different commercial zeolite catalysts for the destruction of technical lignin in water, conducted under atmospheric argon conditions at 300 °C. Therein, Hβ (30) zeolite exhibited the best catalytic cleavage of the C–C bond due to its abundant Brønsted acid sites (0.54 mmol NH_3 g^{-1}) and high specific surface area (621.1 m^2 g^{-1}). Under an inert atmosphere, the protonated hydroxyl group on the aromatic ring was activated over Brønsted acid sites and formed an oxonium ion first; then, the proton was transferred to the adjacent aromatic ring and formed an activated carbocation; a neighboring Csp^2–Csp^3 bond scission occurred (Fig. 6b). The alkylation of C_α to generate alkylphenol carbocation would undergo another scission of the Csp^2–Csp^3 bond, producing another phenol and an aldehyde (ketone) carbocation by adding a H_2O molecule and forming the corresponding alde-

hyde (ketone) by donating the proton back to the Brønsted acid site of Hβ (30) zeolite.[111]

Despite its advantages, HTL often yields modest monomer content, especially from technical lignin.[110,111] Nevertheless, its ability to operate without fossil-derived hydrogen and in a green solvent system positions HTL as a promising route for the sustainable valorization of lignin. Future efforts should focus on lowering operating temperatures, enhancing monomer yields, and developing robust catalysts tailored for aqueous-phase depolymerization.

2.2.2.2 Reductive catalytic depolymerization (RCD) of isolated lignin. Reductive catalytic depolymerization (RCD) involves the processing of isolated lignin in an organic solvent (or its aqueous mixture) with a hydrogen source over a heterogeneous catalyst.[112] Similar to the methods employed in an RCF biorefinery, alcohols with small molecules as solvents are favored owing to their effective lignin solvolysis capabilities.[112] Sahayaraj *et al.*[113] showed the superior performance of ethanol compared to methanol in the solvolysis of corn stover lignin under a hydrogen atmosphere. This superiority was evidenced by a substantial increase in monomer yield and a concurrent decrease in coke formation. At elevated temperatures, effective cleavage of lignin linkages occurred, facilitated by the solvolytic effect, resulting in a reduction of the lignin M_w from approximately 5000 Da to below 2500 Da. However, when subjected to thermal conditions without the presence of a catalyst, monomer yields diminish, and char formation becomes inevitable due to the condensation and repolymerization of reactive intermediates. Sahayaraj *et al.*[114] also systematically explored catalysts for the depolymerization of organosolv lignin in an ethanol solution. Their investigation unveiled that the application of Pd/C at 250 °C and 30 bar H_2, coupled with solvolytic deconstruction, resulted in a significant elevation of volatile content to 83 wt%, concurrently reducing fixed and non-volatile carbon components. The acidic functionalities on bifunctional catalysts can facilitate both lignin interunit–unit cleavage and promote the recondensation and solid catalyst coking processes.[115,116]

The cleavage of β-O-4 linkages usually begins with the dehydroxylation of the C_α–OH bond, forming a radical intermediate (Fig. 6d). This process significantly reduces the C_β–O BDE from 274.0 kJ mol^{-1} to 66.9 kJ mol^{-1}, facilitating its cleavage into styrene, phenols, and ethers using H_2 and an alcohol solvent.[117] In hydrogenolysis systems, the reaction is more likely initiated by the dehydrogenation of the C_α–OH group to form a C_α=O intermediate and predominantly yields acetophenone as one the main product.[118] Nevertheless, β-O-4 models lacking C_α–OH or those possessing the intact β-O-4 skeleton without phenolic hydroxyl and methoxy groups are less susceptible to reductive cleavage.[42] In some cases of condensed lignin, particularly technical lignin, C–C bond cleavage is essential to augment the degree of depolymerization. As demonstrated in the report of Kong *et al.*,[111] the cleavage of inter C–C linkages in conjunction with the disruption of C–O bonds of condensed lignin can yield additional monomers ranging from 7% to 10%. The cleavage of C–C bonds generally
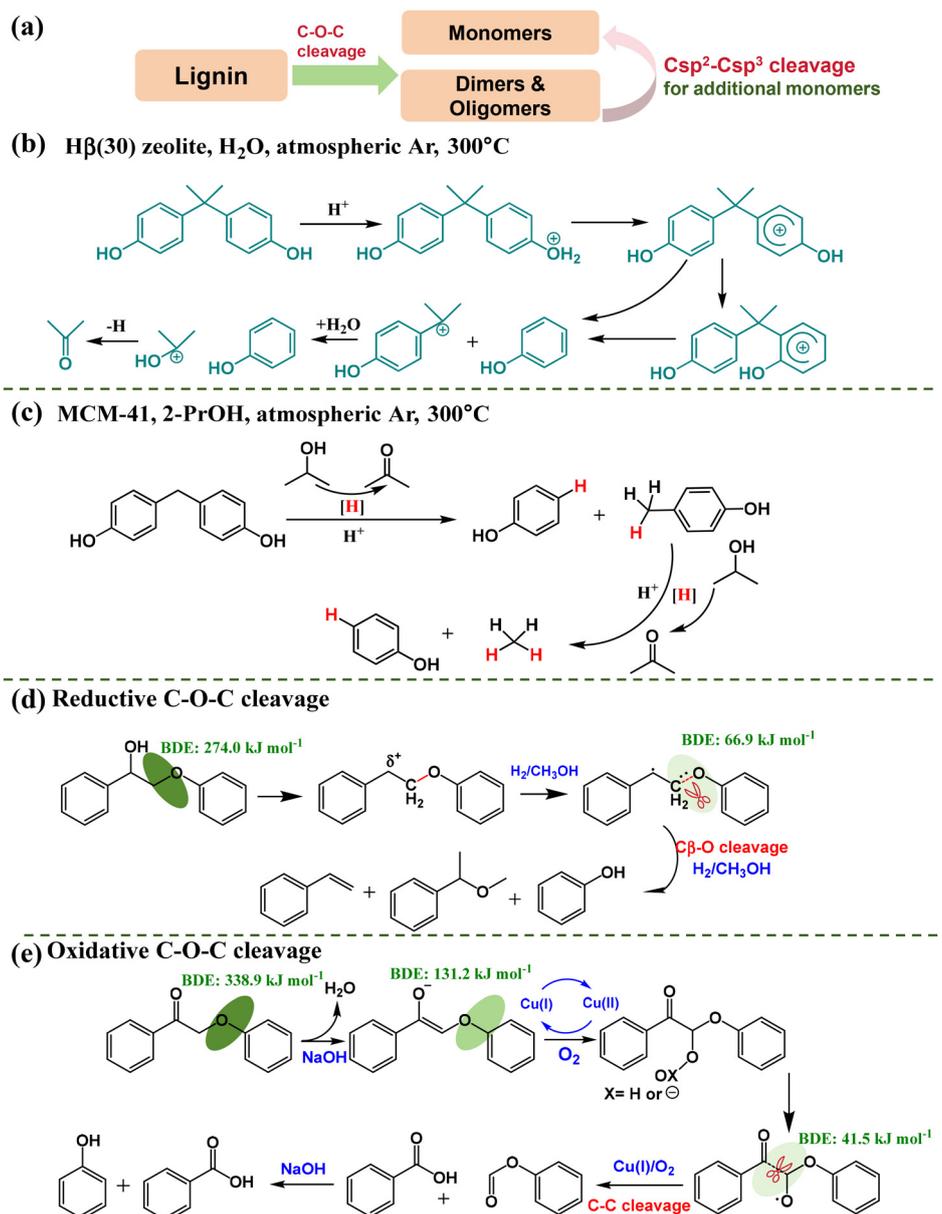
Fig. 6 (a) Scheme depicts two steps of lignin depolymerization aimed at enhancing the yield of monomers. (b) Interunit C−C linkage cleavage in aqueous solution over Hβ (30), reproduced from ref. 111 with permission from the American Chemical Society, copyright 2023, and (c) isopropanol (2-PrOH) solution over MCM-41, reproduced from ref. 122 with permission from John Wiley and Sons, copyright 2024. (d) Interunit β-O-4 linkage cleavage of a model dimer in reductive depolymerization over a NiMo sulfide catalyst in methanol under 1.0 MPa H$_2$ and 180 °C, reproduced from ref. 117 with permission from the Royal Society of Chemistry, copyright 2016. (e) Oxidative depolymerization over CuCl salt in aqueous NaOH under 1 atm and 30 °C, reproduced from ref. 131 with permission from the Royal Society of Chemistry, copyright 2021.

occurs at acidic sites of catalysts, commonly zeolites,[119] whereas conventional Ru/C and Pt/C have a limitation on the cleavage of C–C.[120] However, if acidic C–C scission is poorly controlled, it may lead to undesirable condensation reactions.[121] Kong *et al.* proposed a two-step method to depolymerize Kraft lignin (Fig. 6a).[122] This process involved the alcoholysis of C–O–C bonds in isopropanol (2-PrOH) without a catalyst, followed by the addition of a commercial MCM-41 zeolite for C–C cleavage in the same pot. Complete alcoholysis yielded an 8.9% monomer and a 12.9% dimer, and subsequent selective

cleavage of C–C linkages over MCM-41 zeolite produced an additional 4.0% monomer and 6.2% dimer under optimized conditions. MCM-41 with 2-PrOH under an inert atmosphere selectively supported the hydrogenolysis of the α-5′ bond of bisphenol F (Fig. 6c), but not the 5–5′ bond of 4,4′-biphenol and the β-1′ bond of 4,4′-(ethane-1,2-diyl) bis(2-methoxyphenol). Shuai *et al.*[120] also documented a comparable selective cleavage mechanism.

Currently, most reports on RCD focus on the cleavage of the β-O-4 bond, with limited research on C–C bond cleavage,

especially the 5–5 and β-5 bonds, due to their high dissociation energies.[123] Aromatics connected by C–C linkages without vicinal phenolic hydroxyl groups on the ring are highly challenging to cleave over zeolites or traditional metallic catalysts (*e.g.*, CoMo/Al$_2$O$_3$ and MoS$_2$) because they lack acceptors for protons donated by Brønsted acids[111] or electrons.[120] However, Dong *et al.*[124] reported that using NbOPO$_4$ as a catalyst carrier might address these challenges. Both benzene rings of biphenyl were initially adsorbed onto Ru/NbOPO$_4$ in parallel, leading to their protonation and the formation of intermediate carbocations. Hydrogenation of one benzene ring of biphenyl occurred rapidly in the presence of hydrogen, yielding phenylcyclohexane adsorbed on the catalyst *via* its phenyl group, thereby shifting from Csp^2–Csp^2 to Csp^2–Csp^3 in the 5–5 linkage.[125] Subsequently, 5–5 linkages were easily disrupted, and the resulting volatile products readily desorbed from the catalyst surface.

Alcohol solvents can substitute the external hydrogen gas supply, as they concurrently function as an *in situ* hydrogen source. However, using a pure alcohol solvent is prone to depletion and promotes side reactions over the catalyst during RCD.[122] An organic-water mixed or pure water solvent emerges as a more environmentally appealing alternative. Feng *et al.*[115] clarified that, in an inert atmosphere, the depolymerization efficiency of lignin with the Ni–Al/MCM-41 catalyst in ethanol (EtOH) surpassed that achieved with water and methanol. Matsagar *et al.*[126] employed formic acid as a hydrogen source to deconstruct alkali lignin over Rh/C in various EtOH/H$_2$O co-solvents. Herein, the co-solvent exhibited an excellent depolymerization effect, attributed to its superior solvolytic effect on lignin. Isolated lignin features methoxy groups in aromatic units, and aliphatic hydroxyl groups can serve as sources for *in situ* hydrogen generation.[127,128] Li *et al.*[128] have demonstrated the potential of self-generated hydrogen by depolymerizing four types of lignin/lignin oil (from birch, poplar, camphor, and beech) without external hydrogen over Pt/NiAl$_2$O$_4$ in water, under conditions of 250 °C and 2 MPa N$_2$. The mass and molar yields of 4-alkylphenols were observed to be beyond 9.9% (relative to the lignin feed) and 43.9% (among all detected monomeric products), respectively. Without an external hydrogen supply, the C$_\gamma$–OH and C$_\alpha$H–OH in lignin would initially generate hydrogen *via* dehydrogenation and decarbonylation. Subsequently, the *in situ* hydrogen would initiate the reductive depolymerization of lignin *via* β-O-4 bond cleavage and the hydrogenolysis of methoxy groups in the aromatic structure for *in situ* methanol generation. Methanol produced *in situ* will accelerate the process because more hydrogen is generated through aqueous phase reforming (APR) over metal-loaded catalysts.[128] With no additional hydrogen sources, this strategy is promising, and many other catalytic schemes are also being designed.[129,130]

2.2.2.3 Oxidative catalytic depolymerization (OCD) of isolated lignin.

Oxidative depolymerization (OCD), a process with significant potential, can advantageously undergo mild conditions. This intricate configuration involves catalysts such as MoO$_3$/Al$_2$O$_3$,[132] Ni$_{0.75}$Co$_{0.75}$@CsPMo,[133] Cs$_3$H$_2$PMOV$_2$O$_{40}$,[134]

co-catalysts like ligands for metal salts,[131] solvents such as H$_2$O,[132] alcohol[135] and alcohol-H$_2$O,[133] and oxidants like O$_2$,[136] H$_2$O$_2$[132] and air.[131] The OCD can produce phenols, aldehydes, ketones, and aromatic acids, depending on the feedstocks and their configuration. Hardwood-derived monomers, characterized by high yields, typically exhibit a pronounced selectivity for syringaldehyde, while softwood-derived monomers tend to favor vanillin.[131,137] Although yielding relatively low amounts, herbaceous plant-derived monomers also show a significant presence of syringic acid.[131,137] The catalytic depolymerization occurs on C$_\gamma$–OH or C$_\alpha$–OH in the β-O-4 structure of lignin macromolecules, resulting in the formation of aromatic aldehydes or aromatic acids.[138] However, the cleavage of C–C bonds on the alkyl side chains to depolymerize lignin has some limitations, including poor selectivity and low product yields, due to the instability of the generated phenolic hydroxy group under oxidative conditions.[139]

OCD can be performed in an acidic,[140] neutral,[133] or basic[131] environment. Alkaline aerobic oxidation is one of the most studied strategies, and typical conditions include temperatures of 130–190 °C, reaction times of 10–180 min, O$_2$ partial pressures of 2–5 bar, and 2 M aqueous NaOH, typically targeting vanillin production.[66] Hu *et al.*[131] developed a streamlined oxidative conversion system utilizing CuCl salt as a catalyst, enabling efficient lignin depolymerization in NaOH solution without complex ligands at 160 °C under 5 bar of air. This approach achieved monomer yields ranging from 22 wt% to 38.6 wt%. Based on the model dimer investigation, the base-catalyzed cleavage of C$_\beta$–H in the β-O-4 or β-1 linkage to form an enolate after dehydrogenation of C$_\alpha$–OH was the rate-limiting step in deconstruction. Subsequently, the enolate underwent oxidation to generate a peroxide intermediate *via* a copper-catalyzed single-electron transfer (SET), followed by cleavage into oxygen-centered radicals over copper (Fig. 6e). This radical could rapidly undergo C–C fragmentation, forming a benzaldehyde radical and an ester, or benzaldehyde. The benzaldehyde radical was ultimately oxidized into benzoic acid, while the ester was easily converted to the final products, phenol and small molecules of carboxylic acid, through hydrolysis in alkaline conditions. The cleavage location of the β-O-4 bond is C$_\alpha$–C$_\beta$ rather than C$_\beta$–O, despite the lower BDE of C$_\beta$–O (81.09 k$_{cal}$ mol^{-1} *vs.* 69.20 k$_{cal}$ mol^{-1}), because the formation of radicals decreased the BDE of C$_\alpha$–C$_\beta$ from 81.09 k$_{cal}$ mol^{-1} to 9.92 k$_{cal}$ mol^{-1}. This finding aligns with the majority of reaction systems reported in other studies.[141–143] However, this mechanism differs from the electrochemical oxidation and base WO$_3$-catalyzed systems reported by Waura-Angkura[144] and Liang,[145] in which C$_\alpha$–OH oxidation precedes C$_\beta$–O bond cleavage, typically leading to the formation of phenols and aldehydes. The location of C–C and C–O cleavage, a crucial aspect of the research, affects the selectivity of the product during depolymerization. Based on the exploration of model dimers, it is well-known that functional groups on the aromatic rings and aliphatic side chains of dimers significantly impact the effectiveness of depolymerization. Similar to reductive depolymerization, a strong electron-donating group on the

aromatic ring of lignin is more likely to promote the oxidative cleavage of inter C–C linkage.[131] For example, the depolymerization efficiency of oxygen ether bonds without hydroxyl groups in the side chain is probably not as smooth as that of C–C bonds containing benzyl hydroxyl groups in the $CuCl_2$/ PBOZ oxidative system.[146]

The configuration of solvent and oxidant is also essential. It is well known that the solvent (*e.g.*, alcohol-water as co-solvent) has a hydrogen bonding force (δ_H) with the hydroxyl groups (phenolic or alkyl hydroxyl), facilitating C_α–C_β cleavage because of deprotonation, and suppressing the lignin fragment recombination.[132] Liang *et al.*[145] used *tert*-butyl hydrogen peroxide (TBHP) as the oxidant to base-depolymerize lignin over nano WO_3 particulate, yielding 80.4 wt% of liquid oil from Organosolv lignin with 91.6 wt% monomeric selectivity. Herein, TBHP, as a green oxidant superior to traditional H_2O_2 and O_2, could react with NaOH and abstract the hydrogen atom to produce a tertiary butyl peroxy anion, then transfer an oxygen atom to nano WO_3 to form a metal peroxide species, facilitating the oxidative conversion of C_α–OH to ketone, prone to suffer a breakage to give guaiacol and *p*-methoxy acetophenone.

2.3 Comparison of different lignin-derived oils

Fast pyrolysis of lignocellulose has been commercialized by companies like Ensyn and Biomass Technology Group (BTG) BV, with over 50 large-scale pyrolysis facilities worldwide,[147] with the Empyro plant in the Netherlands capable of converting approximately 40 000 tons of dry lignocellulosic biomass annually to produce 25 000 tons of biocrude.[107] This biocrude, consisting of pyrolytic lignin and sugar, has a relatively hydrophilic nature, low pH of around 3.0, a water content of around 22.5–42.9 wt%, and elevated oxygen content of approximately 40 wt%, resulting in a low Higher Heating Value (HHV) ranging from 14 to 24 MJ kg^{-1}.[148–150] Reactive species contribute to the limited thermal and storage stability, commonly referred to as aging.[149] The viscosity of fast pyrolysis biocrude can reach roughly 20.67 cSt (at 40 °C),[147] with hardwood-derived oil generally exhibiting lower viscosity than softwood.[151] Catalytic pyrolysis can reduce the oxygen content (from 36.5 wt% to 16.5 wt%) and increase the pH value (from 2.66 to 3.00).[147] However, the catalyst's effect tends to increase the water content in the oil while having a less significant impact on the M_w of the bio-oil.[152,153] The biocrude oil obtained from the HTL method exhibits a lower oxygen content (10–30 wt%), offering superior characteristics such as increased stability, improved miscibility, lower acidity, and higher calorific value.[147,148,154] HTL reduces the energy input required for dewatering and drying, making it compatible with wet biomass conversion and achieving a positive energy balance that pyrolysis and gasification cannot.[155,156] However, the high degree of oxygen removal achieved by both catalytic pyrolysis and HTL comes at the expense of biocrude yield, as part of the carbon is diverted into other product streams, with light gases and coke dominating in catalytic pyrolysis and a considerable portion entering the aqueous phase in HTL.[157,158] Although pyrolysis and HTL have demonstrated success at bench or pilot scales,

they face challenges for industrial applications, including the necessity for specialized reactor and separator designs and substantial capital investments.[156,158]

Biocrude derived from isolated lignin tends to exhibit more favorable properties than those produced directly from raw biomass. For instance, lignin-derived pyrolysis oils have a lower O/C molar ratio (0.15–0.44 *vs.* 0.26–0.53)[159–161] and average M_W (214–379 g mol^{-1} *vs.* 650–750 g mol^{-1}) than lignocellulose-derived oil.[149,162] The application of the advanced RCD process further improves the oil quality, maintaining a similar average M_W (154–474 g mol^{-1}),[163] a lower water content (0.3–0.7 wt%),[164] and a lower O/C molar ratio (0.06–0.09) (Fig. 7a). When using lignocellulose as the starting feedstock, a lignin-first biorefining strategy is highly advantageous. As reported by Cao *et al.*[56] and Jang *et al.*,[165] oil produced from lignin-first biorefinery, comprising 50–60% phenolic species, shows an average M_W of approximately 250 g mol^{-1} and a lower water content of 0.4–0.6 wt%. Additionally, its optimal elemental composition, characterized by an O/C molar ratio of 0.3–0.4 and an H/C ratio of 1.3–1.4 (Fig. 7a), renders it suitable for the downstream HDO process.

The feedstock and the conversion process influence the composition and concentration of phenolic compounds in lignin-derived oil. These properties are critical, as they dictate the oil's suitability as a SAF precursor and govern the severity of the subsequent HDO process. Softwood lignin typically yields guaiacyl-type monomers, hardwood lignin gives syringyl-type monomers, and herbaceous biomass-derived monomers often contain ester and carboxyl groups.[165] In addition to monomers, the oil also contains dimers and oligomers, though their quantification remains challenging and is rarely reported.[166] For SAF synthesis, using a mixture of monomers and dimers is advantageous, as monomers contribute shorter carbon chains while dimers provide longer chains, together spanning the crbon number range required for jet fuel and offering a greater diversity of isomeric structures.[3] As summarized in Table 1, phenolics from pyrolysis and HTL of isolated lignin generally feature short or absent aliphatic side chains. For instance, syringol accounts for 4.0 wt% and 3.8 wt% of the bio-oil from lignin pyrolysis and catalytic pyrolysis, respectively.[153] HTL-derived lignin oil is primarily composed of phenol, guaiacol, vanillin, and 4-vinylphenol.[167] Biocrude from RCF and RCD contains C2–C5 aliphatic side chains and saturated groups, which enhance the stability of phenolic intermediates and facilitate their conversion into jet fuel-range alkanes. This is exemplified in pine RCF oil, where 4-propanol-guaiacol dominates the monomers and 5–5/β-1 structures prevail among dimers.[55] In contrast, the mild conditions of OCF/OCD introduce carboxyl/ester groups, impacting the efficiency and cost of subsequent HDO.[168,169] Therefore, biocrude derived from RCF or RCD holds a distinct advantage. To understand this advantage at a molecular level, the oxygen-containing functional groups in the biocrude from the RCF and RCD is assessed in this section. As shown in Fig. 7b and c, the abundant Ph–OH and Ar–OMe groups will compete for adsorption on the catalyst surface, which may consequently
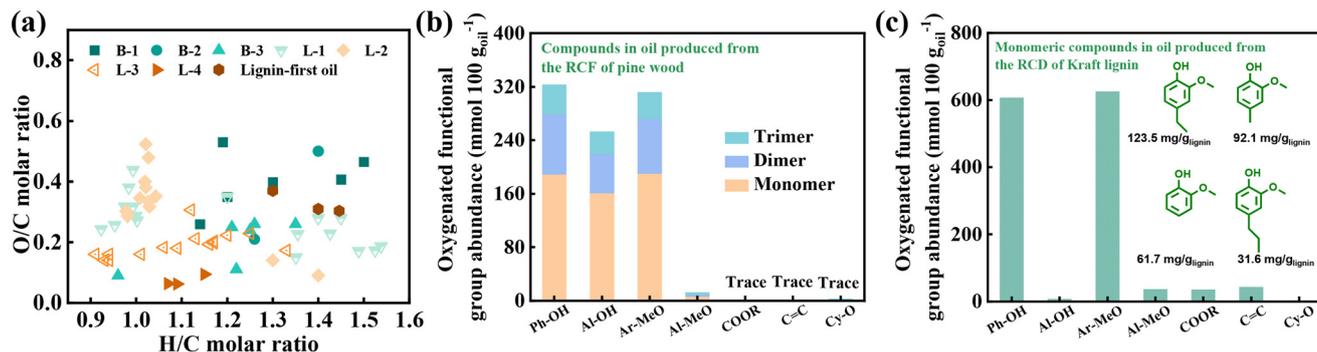
Fig. 7 (a) The molar elemental composition (dry basis) of various bio-oils, with data compiled from ref. 3 with permission from Elsevier, copyright 2022; ref. 159 with permission from American Chemical Society, copyright 2013; ref. 160 and 161 with permission from MDPI, copyright 2019 and 2024; ref. 180 with permission from American Chemical Society, copyright 2016; ref. 181 and 182 with permission from Elsevier, copyright 2022 and 2015; ref. 183 and 184 with permission from the American Chemical Society, copyright 2023 and 2017; ref. 185 with permission from Elsevier, copyright 2020; ref. 186 with permission from the Royal Society of Chemistry, copyright 2014; ref. 187 with permission from MDPI, copyright 2020; ref. 188 with permission from the American Chemical Society, copyright 2017; ref. 189 with permission from MDPI, copyright 2025. B-1 is lignocellulose fast pyrolysis oil; B-2 is lignocellulose catalytic pyrolysis oil; B-3 is lignocellulose HTL oil; L-1 is lignin fast pyrolysis oil; L-2 is lignin catalytic pyrolysis oil; L-3 is lignin HTL oil; L-4 is lignin catalytic depolymerization oil. Abundance of oxygen-containing functional groups in lignin-derived oils produced via (b) RCF of pine, calculated from identified monomers, dimers, and trimers, with data compiled from ref. 55 with permission from the Royal Society of Chemistry, copyright 2022, and (c) RCD of Kraft lignin, quantified based on measured monomers only (insets illustrate the concentrations of predominant monomers), with data compiled from ref. 190 with permission from Elsevier, copyright 2023.

increase the propensity for coke formation during HDO.[170,171] To suppress coke formation, future strategies should therefore focus on the rational design of both catalysts and HDO reaction conditions.[172,173]

3. Upgrading lignin-derived oil to hydrocarbons

The oxygen in lignin-derived oil exists as oxygen-containing functional groups, which are highly undesirable due to their low chemical stability, increased acidity, low calorific value, corrosion of metallurgy, and poor compatibility with standard infrastructure materials.[191,192] The highly reactive oxygen-containing groups can induce polymerization between molecules, resulting in the formation of gums, acids, and other impurities during storage. The upgrading methods include emulsification, solvent addition, hydrotreatment, and catalytic cracking.[33] The most widely adopted and well-established method for upgrading bio-oil is catalytic HDO, a process that effectively removes oxygenated compounds from bio-oil, thereby enhancing its quality and improving its compatibility with existing refinery infrastructure. This process includes hydrogenation, dehydration, deoxygenation, demethoxylation, demethylation, and cracking.[193] It aims to eliminate the oxygenates from bio-oil and retain the carbon number of the bio-oil.[193] The oxygenates typically exist in C_{aryl}–O–C_{alkyl}, C_{alkyl}–O, C_{aryl}–OCH$_3$, C_{aryl}–OH, and C=O in the lignin-derived oil.

3.1 Overview of the hydrodeoxygenation (HDO) process

Research on the HDO process often starts with model oxygenates to elucidate the catalytic cleavage pathways of oxygen-containing groups. As shown in Table 2, model monomers, such as phenol, guaiacol, vanillin, and eugenol, are commonly used due to their simplicity and ease of tracking.[194,195] However, research on model dimers is relatively limited, with a focus on 4-benzyloxyphenol, diphenyl ether, 2,2′-bisphenol, and biphenyl.[195–198] Fig. 8 presents the potential HDO conversion pathways of typical monomers and dimers. The HDO behavior of these phenols is intricately linked to their quantities and distribution of oxygenated groups.[23] Monomers with complex oxygenated group distribution (e.g., vanillin) will form a steric effect, hindering their complete deoxygenation.[199] Dimers exhibit greater sensitivity to temperature than monomers, and an excessively high reaction temperature can result in the loss of dimers in the ungraded product.[3] Additionally, the characteristics of the catalyst impact the conversion of dimers. Reduced Brønsted acidic sites on a catalyst (e.g., NiMo/γ-alumina) can promote higher yields of dicyclic alkanes by facilitating moderate dehydrogenation pathways towards dibenzofuran.[196] Numerous essential HDO mechanisms for various model compounds have been comprehensively documented in multiple articles.[23,200,201]

3.2 Strategies for enhancing selectivity during hydrodeoxygenation (HDO)

The transformation of aromatic oxygenates into cycloalkanes, a vital objective of the hydrogenation-deoxygenation (HYD) procedure, is significant. This transformation begins with the hydrogenation of the benzene ring, followed by the hydrogenolysis of the C_{alkyl}–OAr linkages, representing the rate-limiting step in the HDO process—the saturation of the aromatic ring aids in diminishing the strength of the C_{aryl}–O bond.[194] HDO can alternatively occur through a direct route (DDO), where the initial step involves cleaving the C_{aryl}–O bond, followed by

Table 1 Yield and composition of phenolic compounds in lignin-derived oils

Feedstock	Catalyst	Method	Yield of oil (basis)	Concentration of phenolics (basis)	Key phenolic compounds	Ref.
Hydrolysis lignin (Aspen)	—	Fast pyrolysis	61 wt% (lignin)	Total phenolics 12.5 wt% (oil)	4-Methoxy-3-(methoxymethyl)-phenol (1.5 wt%), guaiacol (1.7 wt%), syringol (4.0 wt%), oil basis	153
Hydrolysis lignin (Aspen)	Zeolite	Fast catalytic pyrolysis	56 wt% (lignin)	Total phenolics 14.6 wt% (oil)	Methyleugenol (2.7 wt%), syringol (3.7 wt%), 4-methoxy-3-(methoxymethyl)-phenol (2.0 wt%), oil basis	153
Poplar	CuO/CeO$_2$	RCF	—	Monomers 31.4 wt% (lignin)	Dihydrosinapyl alcohol (10.4 wt%), dihydroeugenol (6 wt%), propylsyringol (4.7 wt%), lignin basis	174
Wheat straw	CuO/MgAlO$_3$	RCF	—	Monomers 10.3 wt% (lignin)	Methyl 3-(4-hydroxyphenyl) propanoate (6.8 wt%), methyl 3-(4-hydroxy-3-methoxyphenyl) propanoate (3.5 wt%), lignin basis	175
Pine	Ru/C	RCF	42.5 wt% (lignin)	Monomers 13.0 wt% (lignin)	Propyl-guaiacol (5.0 wt%), propenyl-guaiacol (3.8 wt%), propanol-guaiacol/vanillin (3.9 wt%), lignin basis	165
Poplar	Ru/C	RCF	65.1 wt%, (lignin)	Monomers 32.6 wt% (lignin)	Propyl-guaiacol (9.8 wt%), propyl-syringol (8.1 wt%), lignin basis	165
Corn stover	Ru/C	RCF	81 wt% (lignin)	Monomers 32.1 wt% (lignin)	Methyl-dihydrocoumarate (11 wt%), methyl-dihydroferulate (9 wt%), lignin basis	165
Birch	Ni/AC	RCF	18.9 wt% (biomass)	Monomers 46.5 wt%, dimers 49.0 wt% (lignin)	4-Propyl syringol (16.2 wt%), 4-propyl guaiacol (13.9 wt%), lignin basis	176
Pine	Pd/C	RCF	21–22 wt% (biomass)	Monomers 34.0 wt%, dimers 15.8 wt%, trimers 7.3 wt% (oil)	4-Propanolguaiacol (29.0 wt%), β-5 γ-OH (2.8 wt%), oil basis	55
Birch	Ru/C	RCF	—	Monomers 41.4 wt%, dimers 4.87 wt% (lignin)	4-Propyl guaiacol (10.9 wt%), 4-propyl syringol (23.5 wt%), β-5 (3.5 wt%), lignin basis	177
Birch	CuMnCeO$_2$	OCF	—	Monomers 60 wt%, dimers 25 wt%, trimers 9 wt% (oil)	vanillin (6.1 wt%), syringaldehyde (8.2 wt%), vanillic acid (7.6 wt%), lignin basis	168
Hydrolysing lignin (Poplar)	—	OCD	77.6 wt% (lignin)	Monomers 19.3 wt% (lignin)	4-Methylguaiacol (1.0 wt%), acetovanillone (1.5 wt%), eugenol (0.8 wt%), lignin basis	169
Enzymatic lignin (Corncob)	NiMg/HAP	HTL	—	Monomers 5.3 wt% (lignin)	Phenol (3.2 wt%), guaiacol (1.5 wt%), lignin basis	178
Poplar lignin	—	HTL	67.0 wt% (lignin)	Monomers 11.6 wt% (lignin)	Phenols (2.9 wt%), guaiacols (2.3 wt%), vanillins (2.1 wt%), lignin basis	167
Pine lignin	—	HTL	66.8 wt% (lignin)	Monomers 7.2 wt% (lignin)	Guaiacols (2.5 wt%), vanillins (2.2 wt%), lignin basis	167
Grass lignin	—	HTL	78.6 wt% (lignin)	Monomers 14.3 wt% (lignin)	4-Vinylphenol (9.4 wt%), phenol (1.3 wt%), lignin basis	167
Kraft lignin (Eucalyptus)	Ni/C	RCD	—	Monomers 4.2 wt% (lignin)	Homosyringic acid (0.87 wt%), syringol (0.44 wt%), propylguaiacol (0.43 wt%), lignin basis	179
Kraft-LignoBoost "BioPiva 100" (Pine)	Ni/C	RCD	—	Monomers 2.2 wt% (lignin)	Propylguaiacol (0.64 wt%), ethylguaiacol (0.36 wt%), lignin basis	179
Kraft lignin (Pine)	Pt/C	RCD	—	Monomers 5.1 wt% (lignin)	Propylguaiacol (2.7 wt%), ethylguaiacol (0.7 wt%), lignin basis	179
Soda lignin (Wheat straw)	Ni/C	RCD	—	Monomers 4.9 wt% (lignin)	Ethylguaiacol (0.68 wt%), acetosyringone (0.56 wt%), homosyringic acid (0.53 wt%), lignin basis	179
Soda lignin (Birch)	Ru/C	RCD	70 wt% (lignin)	Monomers 44 wt%, dimers 27 wt%, trimers 16 wt% (oil)	Syringol (1.9 wt%), 4-methylsyringol (1.5 wt%), oil basis	112

saturating the benzene ring *via* hydrogenation. This process typically results in the formation of aromatic hydrocarbons.[23]

Enhancing the selectivity of HDO products (cycloalkanes or arenes) is a complex process that often begins with adjusting reaction parameters or precisely designing catalysts. Achieving high selectivity for cycloalkane can result from performing HDO under high H$_2$ pressure at a low temperature. Conversely, low H$_2$ pressure with high temperature favors arenes. The design of the catalyst plays a crucial role in determining product selectivity, with parameter adjustment as a subsequent optimization approach. Therefore, the following discussion will delve into the intricate details of achieving high selectivity in HDO through catalyst design.

3.2.1 Strategies of enhancing selectivity for cycloalkanes

3.2.1.1 Synergistic effect between acidic and metal sites. The selectivity toward cycloalkanes is highly sensitive to the precise

Table 2 Recent reports of HDO of lignin-derived model compounds

Catalyst	Condition	Model compound	Conversion rate	Yield	Selectivity	Ref.
$Fe_{10}Ni_1$/h-BN (10%)	3 MPa H_2, 300 °C, 120 min, decalin	Guaiacol	>98%	Cycloalkane (15.9%)	Cycloalkane (98.4%)	205
Ni_1/β-Mo_2C	4 MPa H_2, 260 °C, 2 h, n-undecane	Dihydroeugenol	100%	Alkane (100%)	Propyl-cyclohexane (100%)	206
Pt/γ-Al_2O_3	4 MPa H_2, 320 °C, 6 h, decalin	Guaiacol	100%	Hydrocarbons (25%)	—	207
Pt/$Nb_xAl_2O_3$	4 MPa H_2, 320 °C, 6 h, decalin	Guaiacol	100%	Hydrocarbons (25%)	—	207
Ni13%/HZ-5 (25)	5 MPa H_2, 160 °C, 2 h, n-undecane	Benzyloxybenzen	100%	Methylcyclohexan (88.9%mol)	—	208
Ni15%/HZ-5 (25)	5 MPa H_2, 160 °C, 2 h, n-undecane	Oxydibenzene	100%	Cyclohexane (79.9%mol)	—	208
Ni/Nb_2O_5–H	20 bar H_2, 240 °C, 1 h, decane	Anisole	46.7%	Benzene (4.1%), cyclohexane (34%), methoxycyclohexane (5.1%)	Deoxygenated products (81.6%)	209
$Pt_{0.4}$/CsPW–H_2	3 MPa H_2,150 °C, 4 h, dodecane	4-Propylguaiacol	95%	Propylcyclohexane (92.3%)	Propylcyclohexane (94%)	210
Co/NC-T-1 : 4	3 MPa H_2, 300 °C, LHSV^a 12 h^{-1}, H_2/oil volume ratio 500 : 1	Eugenol	100%	—	Propylcyclohexane (98.4%)	211
Ni–Cu/SiO_2	1 atm H_2, 350 °C, H_2/m-cresol 50, TOS^b 30 min	m-Cresol	95.2%	Aromatics (90.4%)	Toluene (71.9%)	212
Mo (20 wt%)/ nano γ-Al_2O_3	12 bar H_2, 623 K, WHSV$^{-1\ c}$ 0.333 $g_{cat} \times$ h $g_{4\text{-methylanisole}}^{-1}$	4-Methylanisole	98%	Toluene (41.3%)	Toluene (44%)	213
Fe_2P	0.1 MPa H_2, 200 °C, H_2/anisole 50, WHSV 4.7 h^{-1}	Anisole	100%	—	Arene (96.7%)	214

^{a} LHSV – liquid hourly space velocity. ^{b} TOS – time on stream. ^{c} WHSV – weight hourly space velocity.

tuning of acidic and metallic sites in bifunctional catalysts. This regulation, which optimizes total acidity and strategically modulates the distribution and strength of acidic sites, represents a crucial technical aspect of the process. Such modifications can be achieved through the selection of acidic supports, incorporation of organic or inorganic acids, acid treatment, or the introduction of oxophilic metals.[215–217] The acid modification and introduction of oxophilic metals offer advantages with more stable acidic sites and synergistic effects from metal sites. Phosphotungstic acid (PW) modifying Ru/C exhibited a higher selectivity for cyclohexane than Ru/C-Al_2O_3 during HDO guaiacol due to more acid sites over Ru/C-PW (11.58 μmol g^{-1}).[195] Modifying Ni/NbO_x with Co increased the proportion of Brønsted acids because the decreased amount of Ni and Co cations results in fewer Lewis acid sites, which can accelerate the cleavage of the C_{alkyl}–OH linkages of intermediates.[218] Excessive acidic sites achieve a higher conversion rate at the initial stage of the reaction. However, they exacerbate coke formation, eventually covering active sites and diminishing HDO activity as the reaction proceeds.[219] A desired catalyst must have both Brønsted and Lewis acidic sites. Brønsted acid sites facilitate the conversion of cyclohexanol intermediates to cycloalkanes, and they also adsorb oxygen atoms from phenolics, followed by supplying protons to weaken C_{aryl}–OH bonds.[35] Higher Brønsted acid sites usually have higher dehydration activity.[220] Lewis acid plays an auxiliary role in the HDO process.[35] To illustrate, the Ni–Mo catalyst resulted in the highest proportion of weak Lewis acidic sites compared to the

$NiMo/SiO_2$ catalyst, which facilitated a lower activation energy for HDO and mitigated coke formation.[221] Many reports emphasize rationalizing the ratio of Brønsted/Lewis acid sites. Chen et al.[216] used 4-trifuoromethyl salicylic acid (TFMSA) to modify Ru/γ-Al_2O_3 and achieved an increased ratio of Brønsted/Lewis acid, which resulted in a 95.32% selectivity of cyclohexane from HDO of phenol. Given that the dehydration of cyclohexanol to cyclohexene was a rate-limiting step, the carboxyl group (–COOH) on the TFMSA remarkably promoted cleavage of C_{alkyl}–O linkage due to the reduction of breaking barrier energy varying from 1.74 eV to 1.42 eV compared to the clean Ru (101) (Fig. 9a).[216] In contrast, the Ni_2Al_1-re460 material prepared by Jiao et al. lacks Brønsted acid sites but has an abundance of Lewis acid sites.[222] It achieves nearly 100% conversion of phenolic compounds with high selectivity for cyclic alkanes. Too strong or weak acidity is unpreferred.[35,219,223] Li et al.[221] pointed out that the $NiMo/SiO_2$ with more weak acidic sites than $CoMo/SiO_2$ and NiW/SiO_2 revealed the highest selectivity for cycloalkanes. Wu et al.[223] used FeO_x to modify $Ni_3Al_3O_x$ and achieved the desired medium acidic strength for a high conversion and cycloalkane selectivity. Although excessive FeO_x increased the density of strong acidic sites and maintained cyclohexane selectivity, it exhibited a low guaiacol conversion rate (20.35%). Duan et al.[220] found that Pd/P_2O_5/SiO_2 with higher Brønsted acid sites had a low HDO activity due to weak Brønsted acid strength.

Acidic sites are not a single factor; metal sites are also essential. Generally, small metal particles with rich reduced
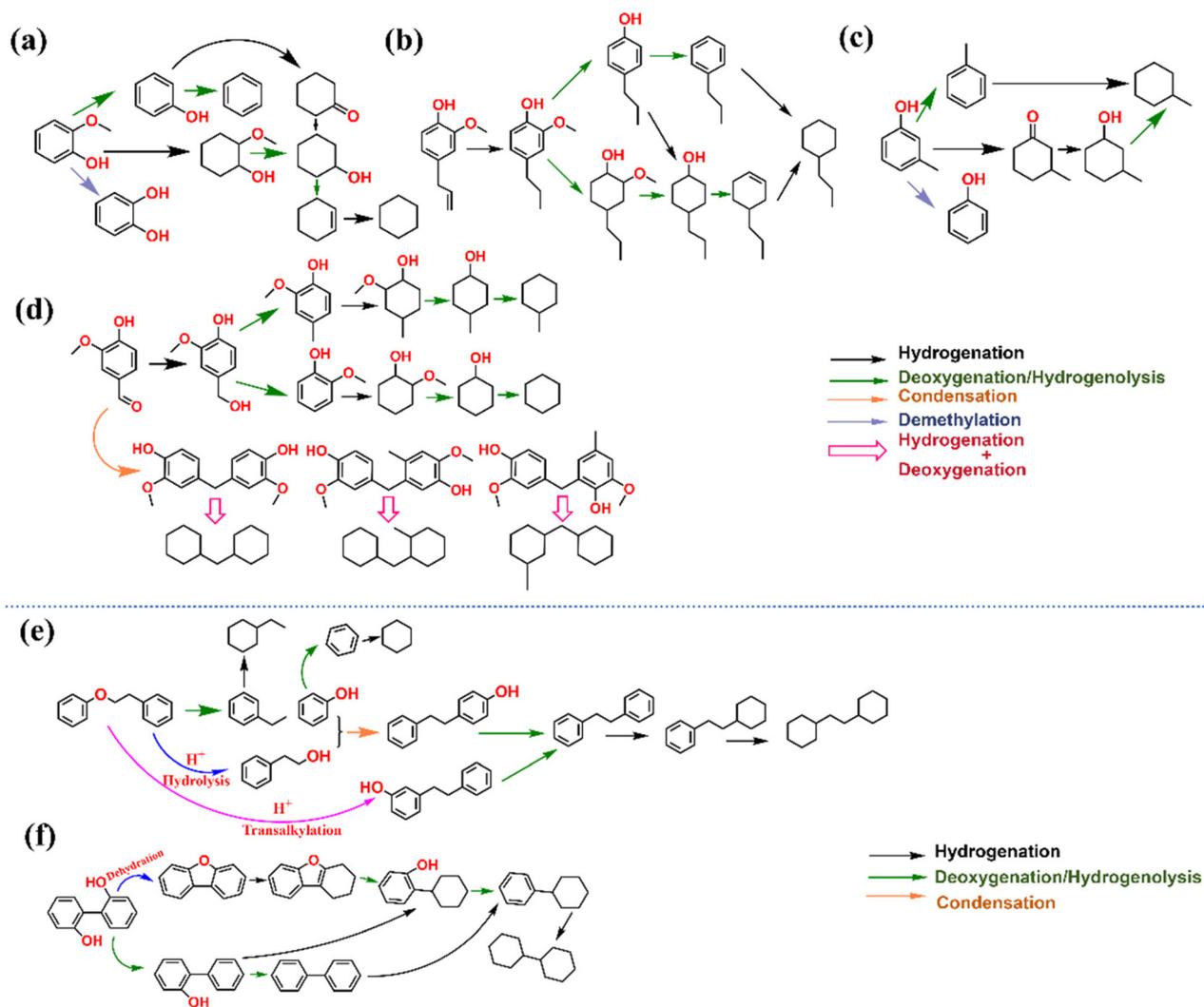
Fig. 8 Proposed HDO pathways of typical monomers and dimers, including (a) guaiacol, adapted from ref. 200 with permission from Royal Society of Chemistry, copyright 2020; (b) eugenol, adapted from ref. 202 with permission from Royal Society of Chemistry, copyright 2015; (c) *m*-cresol, adapted from ref. 200 with permission from the Royal Society of Chemistry, copyright 2020; (d) vanillin, adapted from ref. 203 and 204 with permission from Elsevier, copyright 2022 and 2016, respectively; (e) 2-phenethylphenylether; and (f) 2,2′-biphenol, adapted from ref. 196 with permission from the Royal Society of Chemistry, copyright 2020.

metallic species enhance HDO activity and selectivity.[222] However, larger metallic particles with terrace sites favor the HYD and hydrogenolysis (HYG) pathway, while smaller particles with edges and corner sites favor the DDO pathway.[224,225] As reported, more ring hydrogenation and subsequent ring-opening products were formed over larger-sized Ru/TiO$_2$ catalysts, due to aromatics being more favorable for adsorption on well-coordinated Ru terrace sites *via* an upright configuration.[226] In contrast, smaller-sized Ru/TiO$_2$ catalysts are preferred for arenes production because of adsorptions of aromatic adsorbates *via* upright configuration on under-coordinated Ru sites.[226] Mortensen *et al.*[227] summarized that Ni particles smaller than 9–10 nm are favorable for deoxygenation, while those larger than 10 nm are more favorable for hydrogenation. Yang *et al.*[225] pointed out that high Ni loading

(15.7 wt% Ni/Beta; d_{Ni} = 9.2 nm) can form a Ni cluster with the (100), (110), and (111) surfaces, which favors cycloalkane production due to the reduction of the activation energy of H$_2$ dissociation at low temperature (230 °C). Numerous documents also attribute high selectivity to the proximity between the two types of active sites.[200] However, the intimacy does not imply "the closer, the better".[200] As emphasized by Ju *et al.*,[228] the distance between acid and metal sites at the nanoscale (Pt dispersed on the Al$_2$O$_3$ part of the Al$_2$O$_3$-ZSM-5 mixture) could form an optimal selectivity for cycloalkane compared to a closer scale.

Overall, regulating acidity/metal sites and their distances aims to achieve a satisfactory synergistic effect for hydrogenation and deoxygenation. These three factors interact, whereby acidic sites on the support can control the size and distribution of
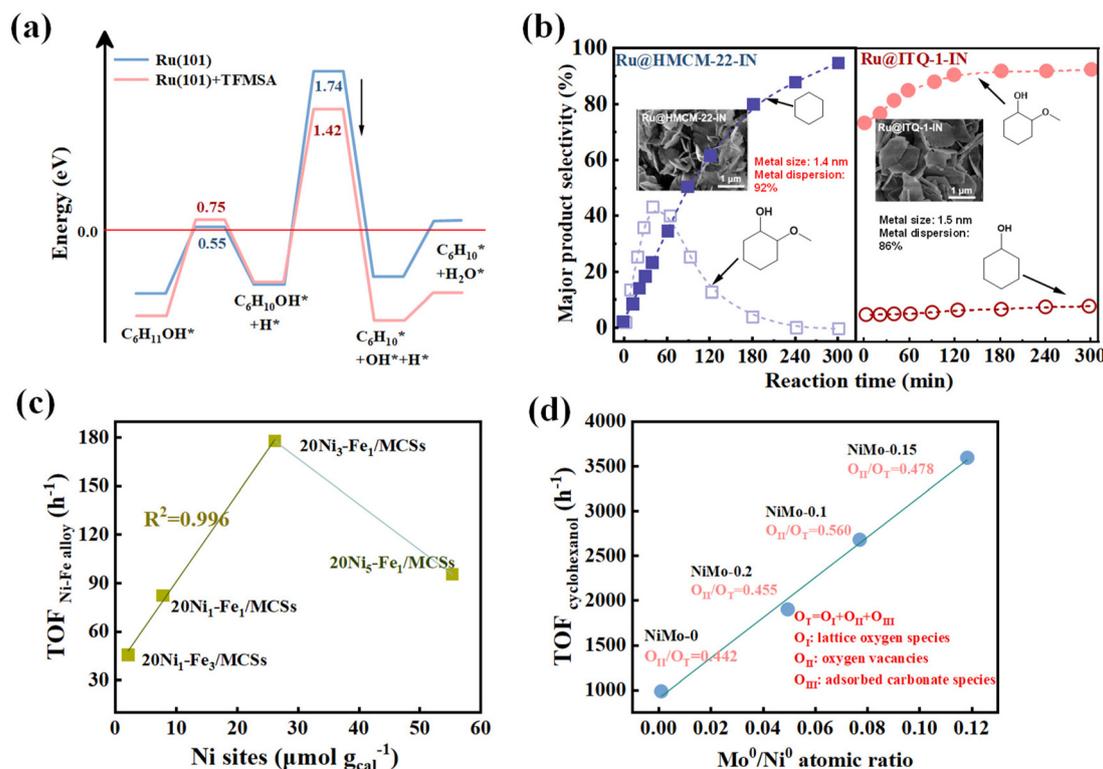
Fig. 9 Enhancing the synergistic effect between metallic and acidic sites to increase cycloalkane selectivity. (a) Carboxyl group modification to increase the Brønsted acid/Lewis acid over $Ru/\gamma-Al_2O_3$, adapted from ref. 216 with permission from Elsevier, copyright 2022. (b) Achieving proximity between Ru metal clusters and Brønsted acid sites over Ru@HMCM-22-IN, adapted from ref. 229 with permission from the American Chemical Society, copyright 2022. (c) Optimization of Ni/Fe ratio of bimetallic catalyst, adapted from ref. 242 with permission from Elsevier, copyright 2019. (d) Tuning of O_V (O_{II}/O_T ratio) over Ni-Mo catalyst for enhancing hydrogenolysis of cycloalkanol, adapted from ref. 231 with permission from the American Chemical Society, copyright 2021.

metal particles, thereby collectively determining the relative distance between them. However, the porous structure of the support also needs consideration, as microscopic pores can limit the diffusion of reactants and their accessibility to active sites. He et al.[229] proposed to confine the sub-nanometric Ru metal clusters in MWW-type zeolite (Ru@HMCM-22-IN) to achieve proximity between Ru metal clusters and Brønsted acid sites in zeolite constraints. Fig. 9b depicts product selectivity during the HDO of guaiacol. The structure of Ru@HMCM-22-IN endows a higher HDO activity and cycloalkane selectivity compared to siliceous analog catalysts (Ru@ITQ-1-IN). The strong interrelation between these sites prevents metal particles from sintering and leaching off after multiple uses.[230]

3.2.1.2   Using oxophilic metal as a promoter of a bifunctional catalyst. Careful consideration must be given to the oxophilicity of reducible metals to achieve high selectivity for cycloalkanes. Metals with low oxophilicity, such as Pd, Pt, Ni, and Rh, cannot directly cleave the C–O bond but exhibit significant activity in saturating aromatic rings. In contrast, highly oxophilic metals like W, Al, Nb, and Zr strongly interact with abstracted oxygen yet struggle to release oxygen even in the presence of H_2. Metals with moderate oxophilicity, such as Ru, Fe, Co, and Mo, can effectively abstract oxygen from phenolics and readily eliminate it with the assistance of H_2.

A potential strategy for achieving selective cycloalkanes involves combining metals with high/moderate and low oxophilicity to form bifunctional catalysts, such as Mo–Ni, Fe–Ni, Co–Ni, W–Ru, Pt–Al, and W–Pt, as reported in the literature.[218,221,223,231–234] Hsu et al.[235] reported that for the HDO of p-cresol, the order of cycloalkane selectivity is Ni–W > Ni–Mo > Ni–Fe, which is positively associated with oxophilicity of secondary metal. However, Yan et al. reported a different order of cycloalkane formation rates from guaiacol HDO: Ni–Fe > Ni–Mo > Ni–W.[236] This suggests that doping W may alter the structure of Ni particles, leading to decreased HDO activity.[236] Therefore, in the process of catalyst design, it is essential to comprehensively evaluate the synergistic effect between the two types of metals.

Reducible oxophilic metals, acting as host metal promoters, can modulate the surface electronic environment, activate the hydrogen spillover effect, tune the geometric impact of reactants, and create defects over the catalyst. The electrons can transfer from highly oxophilic metals towards hydrogenation metals, which can localize the charge distribution of the catalyst, decreasing the ΔG_{H*} adsorption to nearly zero, thereby facilitating the hydrogenation performance and activation of the oxygenated groups.[218,237] Oxophilic metal affects the geometric configuration of substrates over catalysts based on the

electronic effect. For instance, phenols can be adsorbed on the Fe(110) surface in parallel by the benzene ring, subsequently distorting the C–O bond, which supports the DDO pathway.[238] The parallel configuration significantly contributes to the hydrogenation of aromatic rings after removing oxygen.[236] Guo *et al.*[206] elucidated that β-Mo$_2$C features a selective tendency to yield arenes because intermediates favor a vertical configuration on the β-Mo$_2$C surface, a state that requires lower free energy. Conversely, on Ni$_1$/β-Mo$_2$C, intermediates tend to be adsorbed horizontally due to the low energy needed, producing cycloalkanes instead.[206] The hydrogen spillover occurring on the reducible oxophilic metal provides additional sites for the hydrogenolysis of C–O bonds and the hydrogenation of substrates.[239]

Moreover, the hydrogen spillover effect between oxophilic and noble metals influences the selectivity of HDO products. As reported by Wang *et al.*,[240] the hydrogen spillover effect became more severe when Pt was loaded onto TiO$_2$ as nanoparticles rather than as single atoms. A weaker hydrogen spillover effect is preferable for promoting demethoxylation while suppressing benzene ring hydrogenation and C$_{aryl}$–OH bond cleavage. In contrast, severe hydrogen spillover tends to drive deep HDO reactions. The hydrogen spillover effect is related to the crystal phase of the oxophilic metal. Hydrogen spillover promoted the HYD over rutile TiO$_2$ mixed with Ru/TiO$_2$, and cycloalkane selectivity was more pronounced than anatase TiO$_2$ mixed with Ru/TiO$_2$.[241] However, Han *et al.*[242] attributed the negative effect of excessive Ni on selectivity to the hydrogen spillover occurring on the Ni–Fe alloy, hindering intermediate-cyclohexanol adsorption (Fig. 9c).

The presence of defects such as O$_V$ originating from oxophilic metal oxides is particularly advantageous. This is because it enhances the cleavage of C–O bonds and synergistically interacts with hydrogenation metals. O$_V$ (strength of M–O bond) is one of the defects of oxophilic metal oxides and serves as a Lewis acidic site. O$_V$ defects can be constructed by hydrothermal, template, sol–gel, solid-phase, and coprecipitation methods.[243] Unlike conventional surface-driven mechanisms, deoxygenation over O$_V$ behavior occurs through a reverse Mars-van Krevelen mechanism. The oxygen atom is removed from the phenolics upon adsorption at the vacancy sites under mild conditions, and the vacancies are then regenerated with H$_2$ to produce water (Fig. 10).[244] Low HDO activity was observed in oxygenated solvents because the strong oxophilicity of the metal could cause competitive adsorption between oxygen-containing solvents and reactants.[245] Zhang *et al.*[231] reported that surface O$_V$ from oxophilic Mo^0 species in the Ni–Mo alloy could improve the C–O cleavage of cyclohexanol. Nevertheless, an improved deoxygenation effect of cyclohexanol does not necessarily coincide with a higher quantity of O$_V$ (O$_{II}$/O$_T$ ratio) (Fig. 9d). The excessive adsorption of cyclohexanol and the destruction of the adsorptive dissociation ability of H$_2$ on the hydrogenation metallic sites resulted in the severe trapping of cyclohexanol on the catalyst surface and inhibited its conversion.[242,246] According to Sun *et al.*,[233] no significant HDO activity over pure WO$_{3-x}$ with O$_V$ under an H$_2$ atmosphere because of the difficulty in releasing the adsorbed
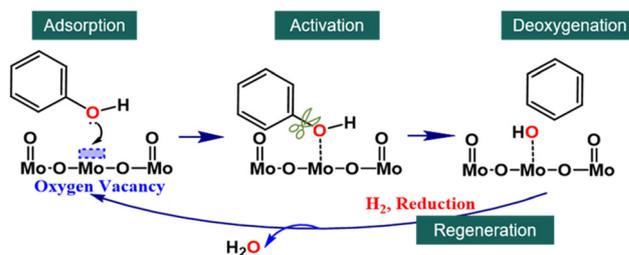

Fig. 10 Deoxygenation pathway of phenol on oxygen vacancies (O$_V$) based on the reverse Mars-van Krevelen mechanism.

oxygen without the metal for hydrogenation. The selectivity for methylcyclohexane surged to 82.9% with the increased presence of Pt^0 species within Pt–WO$_{3-x}$.[233] The dissociated hydrogen atoms would move to the Pt–WO$_{3-x}$ interface through the hydrogen spillover effect, and electrons produced from hydrogen atoms reduced W^{6+} to W^{5+} to form the more active O$_V$ sites.[233] Wang *et al.*[247] further explored the effect of the distance between the metallic sites and O$_V$ on HDO activity. Ni escaped from NiMoO$_4$ through low-temperature hydrogen reduction and was reduced to its metallic state, destroying the NiMoO$_4$ structure. These reduced Ni aggregated together and were located in the neighborhood of the O$_V$ of Mo oxide, which preferred to form a Ni-vacancy interface. The methylcyclohexane selectivity over Ni clusters near the O$_V$ (Ni/MoO$_3$-O$_V$-N) was superior to that away from O$_V$ (Ni/MoO$_3$-O$_V$-F) and on O$_V$ (Ni/MoO$_3$-O$_V$-O). It can be explained that the H$_2$ dissociation capacity of Ni/MoO$_3$ is more robust than that of MoO$_3$. The energy barrier of C$_{alkyl}$–O cleavage on the Ni/MoO$_3$-O$_V$-N was 0.19 eV, obviously lower than 0.88 eV on Ni/MoO$_3$-O$_V$-F and 0.22 eV on MoO$_3$-O$_V$-O.

In summary, increasing total acidity, enhancing the strength of medium and weak acids, and rationalizing the Brønsted/Lewis acid ratio improve the selectivity for cycloalkanes. Larger-sized metal particles are more advantageous for producing cycloalkanes due to the flat adsorption configuration of aromatics over the catalyst. The proximity between acidic and metal sites aids in the accessibility of intermediates to active sites, promoting the C–O bond cleavage of intermediates. Combining metals with high/moderate oxophilicity and metals with high/moderate hydrogenation activity into bifunctional catalysts facilitates optimizing the catalyst surface electronic environment and the geometric configuration of reactants on the catalyst surface. This combination can activate the hydrogen spillover effect and introduce O$_V$ defects on the catalyst surface. These regulatory measures are prospective for precisely controlling the selectivity of cycloalkanes.

3.2.2 Strategies of enhancing selectivity for arenes. The means of selectively controlling arenes are similar to those for cycloalkanes. A high Lewis acid density can enhance the selectivity of arenes.[248] This is attributed to the enriched Lewis acid sites, as these electron-positive centers can favorably adsorb the electron-negative Ar–OCH$_3$ and C$_{aryl}$–O linkages.[249] It has been reported that the arene yield and phenolic com-
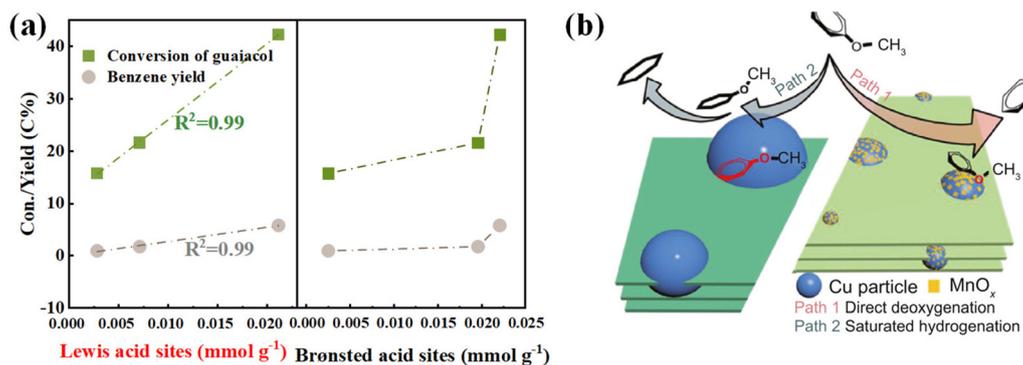
Fig. 11 Strategies for increasing selectivity for arenes. (a) Increasing the Lewis acid density over Ru/HZSM-5, adapted from ref. 250 with permission from Elsevier, copyright 2022. (b) Tuning the adsorption configurations of oxygenate molecules over Cu/MnAlO$_x$, reproduced from ref. 253 with permission from Elsevier, copyright 2023.

pound conversion exhibit a linear relationship with changes in Lewis acid density (Fig. 11a).[250]

As discussed, highly oxophilic metals can decrease the energy barrier for direct C–O bond cleavage while the barrier for hydrogenation increases.[251] Combining highly/moderately oxophilic metals with moderate hydrogenation metals is advisable, as it can decrease the zero-valent hydrogenation metal species and diminish hydrogenation activity. For example, RuFe/Nb$_2$O$_5$ could obtain a mass yield of 8.2% (relative to the lignin oil) with a selectivity of 63.4% ethylbenzene when catalytically deoxygenating birch lignin oil under 250 °C and 4 bar H$_2$.[252] The cleavage site of the C$_{aryl}$–O bond originated from the Fe^{2+}-O$_V$-Nb^{4+} interfacial structure, and the high selectivity towards aromatics was attributed to the direct DDO route facilitated by the synergistic effect of Ru and interfacial NbO$_x$ species. Shao *et al.*[121] investigated the mechanism of DDO over Nb$_2$O$_5$ through calculations of the dissociation energies. The energy required to cleave C–O bonds in pristine phenol was 5.76 eV, and it reduced to 4.41, 5.18, 5.09, and 5.29 eV for adsorbed phenoxide on Nb$_2$O$_5$, ZrO$_2$, Al$_2$O$_3$, and TiO$_2$, respectively. Nb$_2$O$_5$ achieves the most considerable energy reduction (Δ = 1.35 eV) among these four catalysts and facilitates C–O cleavage. Once the C$_{aryl}$–O bonds were cleaved and arenes formed, they were weakly adsorbed. They could desorb from the Nb$_2$O$_5$ surface readily and leave the reaction system rapidly, resulting in an overall unusual selectivity towards the production of aromatics. ZrO$_2$ exhibits strong adsorption of arenes, making it more selective for naphthenes. The adsorption ability of Al$_2$O$_3$ is weaker than that of ZrO$_2$, so the product contains both naphthene and naphthenic oxides. TiO$_2$ has the weakest adsorption and the least promotion effect on C$_{aryl}$–O bond dissociation, so the deoxygenation effect is the worst.

Oxophilic metals further influence the adsorption configuration of reactants. Adjusting the proportion of oxophilic metals can achieve a vertical or tilted adsorption configuration, thereby enhancing selectivity towards aromatic hydrocarbons. Wang *et al.*[253] used MnO$_x$ to modify the surface of Cu particles, facilitating the generation of O$_V$ on the catalyst. It was found that the arenes selectivity obtained on 4Cu/

8Mn$_4$AlO$_x$ was increased to more than six times that on 4Cu/4Al$_2$O$_3$. With the Mn/Cu molar ratio increased, MnO$_x$ tended to cover Cu particles, and an intense interaction formed between them, inhibiting the planar adsorption of aromatic rings over Cu particles.[253] Instead, a tilted adsorption configuration prevailed on the surface of MnO$_x$-modified Cu particles. Consequently, the abundant O$_V$ on MnO$_x$ effectively adsorbed oxygen atoms from anisole, facilitating the production of arenes, which could then be readily released from the catalyst, thereby avoiding further hydrogenation (Fig. 11b).

In summary, increasing Lewis acid/oxophilic sites or coupling strong oxophilic metals with moderately active hydrogenation metals enhances the direct deoxygenation of phenolic compounds while diminishing hydrogenation activity. Similarly, constructing O$_V$ defects promotes the formation of aromatic compounds. By adjusting the type and amount of oxophilic metals, high-efficiency C–O bond cleavage activity can be achieved while maintaining low hydrogenation activity through a non-flat adsorption configuration.

3.3 Green and mild strategies for hydrodeoxygenation (HDO)

Removing oxygen from lignin-derived oil under mild conditions (low temperature and low hydrogen pressure) is a promising but still challenging prospect. The reason is that the high BDE required to break the C$_{aryl}$–O bond (~468 kJ mol^{-1}) and cleavage of the C–O bond is regarded as the rate-determining step of the HDO process. High hydrogen pressure ensured higher hydrogen solubility in the bio-oil and a closer proximity to the catalyst surface, enabling the HDO of phenolic compounds.

As mentioned above, adding hydrogen donors instead of an external hydrogen supply is currently a promising strategy to avoid relying on a high-density hydrogen gas input. Zhang *et al.*[254] compared the effects of an *in situ* hydrogen source (formic acid) and external hydrogen supply on the deoxygenation of lignin-derived pyrolysis oil in supercritical EtOH. Formic acid, acting as a hydrogen donor, facilitates the HDO process without requiring external hydrogen gas input at low temperatures. Moreover, HDO with the *in situ* hydrogen source

could generate more aromatics and hydrocarbons than an external hydrogen gas supply over a Ru/C catalyst under the same conditions.

Except for formic acid, methanol, ethylene glycol, glycerol, sorbitol, and glucose, which can also produce *in situ* hydrogen through catalytic transfer hydrogenation (CTH) and APR routes. Methanol is more sustainable because it can be created from renewable resources such as biomass-derived polyols, sugars, glycerol, or through the demethoxylation of lignin.[255] However, these processes were also accompanied by side reactions with CO_2 and CO formation, which weakened the hydrogen-donating ability and HDO performance.[256] Producing *in situ* hydrogen from inorganic compounds (such as aluminum water) may solve this problem.[257]

An effective hydrogen carrier also has the potential to substitute for high-pressurized hydrogen, facilitating the transfer of H_2 from the gas phase to the liquid phase and thereby enhancing the HDO reaction in the liquid phase. As illustrated in Fig. 12, Liu *et al.*[258] employed a low redox potential polyoxometallate acid, $H_4SiW_{12}O_{40}$ (SiW_{12}), as the hydrogen buffer and carrier. It can quickly transfer hydrogen gas from the gas–liquid interphase into the bulk solution *via* reversible hydrogen extrac-

tion and then release hydrogen as an active species, H*, on the Pt/C surface. The properties of the SiW12-Pt/C system enabled the HDO to proceed under extremely low hydrogen pressure (<1 atm) and simultaneously at a low reaction temperature (<100 °C). The SiW_{12}-associated proton is crucial in significantly decreasing the activation energy (E_a) of the C–O bond breaking in an aqueous solution (Fig. 12). With the super acidic SiW_{12}, the partially hydrogenated phenol can be easily protonated to form an oxonium ion by combining with the hydronium ion H_3O^+ in water. Next, the dehydration of the protonated substrate occurs to yield a carbocation intermediate and water with a smaller activation energy of 97.5 kJ mol^{-1}. This proton-involved mechanism is more energetically favorable.

3.4 Hydrodeoxygenation (HDO) of authentic lignin-derived oil

The HDO of real lignin-derived oil is more complex than that of model compounds. As shown in Table 3, several novel catalysts have demonstrated high conversion rates and selectivity for cycloalkanes during the HDO of lignin-derived oil. The HDO bio-oil products typically consisted of monocyclic, bicyclic, and tricyclic cycloalkanes, along with paraffins and aromatics formed from the monomers, dimers, and trimers of
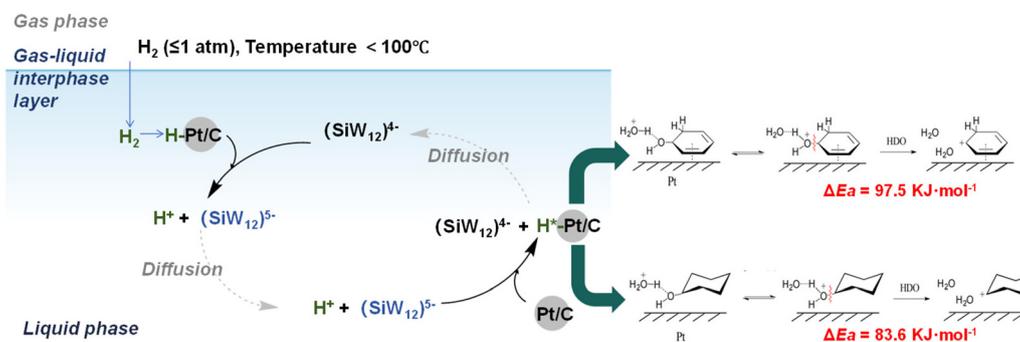

Fig. 12 Proposed reaction pathway of SiW_{12} as a hydrogen buffer over a Pt/C catalyst, and energy profiles of possible C–O bond breaking pathways in phenol and cyclohexanol HDO on a Pt (111) surface with the assistance of SiW_{12}, adapted from ref. 258 with permission from Springer Nature, copyright 2020.

Table 3 Recent reports on deoxygenation of authentic lignin-derived oil

Catalyst	Feedstock	Condition	Product evaluation	Ref.
Ru-NbOPO$_4$	Pyrolysis oil from cornstalk	170 °C, 5 MPa H_2, 10 h, hexane	88.2% yield of hydrocarbons	263
Ni$_1$Mo$_3$N/C	Pyrolysis oil from rice husks	260 °C, 1 MPa H_2, 4 h, octane	88.4% hydrocarbons with 22.9% cyclohexane	264
RuMoO$_x$/AC-1-350	Lignin oil from cornstalk residues hydrogenolysis	280 °C, 30 bar H_2, 5 h, decalin	56.9% hydrocarbons consisting of cyclohexane and alkylated cyclohexane	197
Ni$_2$P–Al$_2$O$_3$(H)$_{71}$	RCF lignin oil from poplar	250 °C, 5 MPa H_2, 15 h, *n*-hexane	98.0% selectivity of alkanes	265
RuCoW$_{0.03}$/NC	Lignin pyrolysis oil	300 °C, 2 MPa H_2, 6 h, *n*-dodecane	19.1% selectivity of aromatic hydrocarbons and 79.3% selectivity of cycloalkanes	266
Ru-HY-60-MI	Lignin oil	220 °C, 1 MPa H_2, 1 h^{-1} WHSV	15.3 wt% cyclohexane, 62.4 wt% alkylcyclohexanes, 11.1 wt% dimers	219
Ni$_2$Al$_1$-re460	Enzymatic hydrolysis lignin (EHL)	320 °C, 2 MPa H_2, 6 h, cyclohexane	128.5 mg g$_{EHL}^{-1}$ cycloalkanes with 100% EHL conversion	222
Pt$_{0.4}$/CsPW–H$_2$	RCF of eucalyptus sawdust	150 °C, 2 MPa H_2, 24 h	32.7 wt% alkanes based on lignin derivatives with 23.3 wt% propylcyclohexan	210

lignin oil. The small quantity of paraffins is likely a result of ring-opening reactions of cycloalkanes at acidic catalytic sites.

For instance, Wang et al.[247] used a Ni-MoO$_3$ catalyst to upgrade lignin-derived oil at 260 °C and 4 MPa H$_2$ for 20 hours in n-hexane. The deoxygenation degree reached 99%, with a remarkable overall carbon yield of 69.4% for naphthenes, including various di-cycloalkanes. The resulting naphthene products primarily fell within the jet fuel range (C6–C18). Compared to model compounds, catalysts in real lignin bio-oil are more susceptible to deactivation due to phenomena such as coking, sintering, and site poisoning.[193] This deactivation typically manifests as blockage, loss, or modification of the catalyst's active sites, which is directly influenced by the feedstock's characteristics, features of the catalysts, and the HDO reaction conditions.[16] Understanding the deactivation behavior of catalysts is beneficial for subsequent catalyst modification, but there are currently limited reports focusing on this aspect.

Nonpolar organic solvents, such as hexane and decalin, are preferred for the HDO of lignin-derived oils because they mitigate mass transfer limitations and reduce catalyst deactivation, thereby enhancing overall process efficiency. Additionally, nonpolar solvents enhance the adsorption of the substrate's aromatic ring structure on the catalyst surface in a parallel orientation, which promotes cycloalkane formation.[259] While water can also serve as a solvent under certain conditions, it typically demands more stringent catalyst requirements. In this context, H$_2$ dissociates into H atoms and forms hydronium ions with water, followed by H transfer to reactants via an H-shuttling mechanism. Verma et al.[260] reported that non-acidic Ru/C, with 7.4% metallic Ru^0 domains and a proportion of partially reduced Ru$^{\delta+}$ sites, facilitated enhanced solvation stabilization of adsorbates, promoting the hydrogenolysis of adsorbed Ar–OH species. Water, as a solvent, offers significant environmental benefits by reducing dependence on fossil fuels; however, this comes with the challenge of maintaining a continuous supply of pure hydrogen, which is essential for the hydrogenation process. Sridharan et al.[261] employed a two-step continuous method to upgrade pyrolysis oil from Kraft lignin, eliminating the need for organic solvents. The first step is performed under 350 °C and 200 bar H$_2$ over a sulfide CoMo/Al$_2$O$_3$ catalyst for stabilization, followed by the second step under 400 °C and 80 bar H$_2$ over a sulfide NiMo/Al$_2$O$_3$ catalyst for deep HDO. After two-step catalytic upgrading, the oxygen content of the final product was reduced to about 0.5 wt%. The main components of the upgraded oil have a median boiling point between 200 and 250 °C, which tails at about 450 °C. The most detected products were cyclohexanes, benzenes, and naphthalenes; their report did not mention di-cycloalkanes. It can be explained that the interunit C–C linkages in lignin were cleaved during pyrolysis, producing rich phenolic monomers.

It is worth noting that arenes, due to their unfavorable combustion characteristics, are typically limited to a maximum of 25% in jet fuels.[25,262] Notably, aromatic structures promoting greater volume swelling do not favor combustion reactivity and soot inhibition, necessitating a trade-off between these properties.[23] Preliminary data suggest that small and lightly substituted C8–C9 aromatics in jet fuel have minimal impact on soot formation while providing seal swelling for backward compatibility.[25] Li et al. reported that RuFe/Nb$_2$O$_5$ exhibited a high selectivity (63.4%) for ethylbenzene from birch lignin oil.[252] Therefore, producing aromatic components as a jet fuel fraction from lignin-derived oil is also feasible.

4. Fuel properties and compatibility challenges

Lignin-derived fuels offer promising potential as SAF candidates owing to their hydrocarbon frameworks, which resemble those of conventional Jet-A (Table 4). Nevertheless, aligning their physicochemical properties with ASTM D7566 standards and ensuring seamless compatibility with existing aviation infrastructure presents ongoing challenges.

Notably, lignin-derived fuels often exhibit high concentrations of multi-cycloparaffins, which are uncommon in conventional jet fuels.[267,268] This skewed carbon distribution toward heavier fractions results in elevated low-temperature viscosities and freezing points, often exceeding ASTM specification limits.[23,268] Despite their presence in Jet-A at around 17 wt%, high levels of bicyclic alkanes in lignin-derived fuels may lead to increased surface tension, diminished ignition performance, and uncertainty in autoignition behavior due to conformational diversity.[268,269] In contrast, low levels of n-/iso-paraffins and aromatics, commonly found in lignin-based SAFs, offer both benefits and drawbacks. While they help satisfy seal swelling requirements without the need for aro-

Table 4 Chemical composition (wt%) of Jet-A and reported lignin derived jet fuel

Chemicals	Jet-A[278]	Report 1[21]	Report 2[268]	Report 3[276]	Report 4[3]	Report 5[266]
n-Paraffin	20.97	8.3	3.89	0.2	2.1	—
iso-Paraffin	30.58	2.44	2.02	5		—
Monocycloparaffin	20.12	33.16	14.42	60.2	5.5^a	79.3
Dicycloparaffin	4.3	34.17	31.95	—		—
Tricycloparaffin		12.41	21.12	—		—
Aromatic	24.05	2.45	—	13.1	87.5^b	19.1
Olefins	0	—	—	—	—	—

^{a} Amount of total cycloalkanes. ^{b} Amount of cycloaromatics (5.5 wt%), diaromatics (1.1 wt%) and alkybenzes (80.5 wt%).

matic blending,[21] they also compromise ignition quality and limit the blend ratio with Jet-A to around 50% by volume.[270] These compatibility issues are central to current SAF certification constraints.

Notably, the molecular structure of cycloalkanes, particularly with respect to branching, geometric isomerism, and ring size, has a significant influence on key jet fuel properties.[23,271,272] As shown in Table 5, alkylated cycloalkanes derived from lignin can achieve high specific energy, energy density, and enthalpy savings, making them promising targets for surrogate jet fuel formulations.[23,271–273] Notably, cycloalkane-rich alkanes possess both a higher smoke point and comparable seal-swelling capability (*e.g.*, 40.8 vol%) relative to conventional jet fuel.[21] Accordingly, precise control of molecular architecture during catalytic conversion is crucial for achieving a balance between performance and compatibility.

To systematically evaluate these attributes, a two-tier prescreening protocol (Tier α and Tier β) has been developed, aligning with ASTM guidelines (Fig. 13). Tier α focuses on predicting combustor-relevant properties from composition and distillation using minimal fuel quantities, while Tier β verifies these predictions through experimental testing. If specific

metrics exceed specification limits, the molecular contributors must be identified and adjusted *via* catalyst or process engineering.[274,275] Unfortunately, comprehensive evaluations of this nature remain scarce and warrant further investigation.

Recent evaluations of neat lignin-derived cycloalkane fuels (LCF) revealed an abundance of light hydrocarbons (C7–C8), contributing to flash points below the ASTM limit (Fig. 14).[276] Furthermore, although the predominance of cycloalkane species results in suboptimal combustion-related metrics compared to conventional jet fuel, these predictions still broadly fall within the specification limits defined by ASTM D7566. The β-tier evaluation of the 10/90 vol% blend of unfractionated LCF and Jet-A (POSF 10325) reveals that the presence of high concentrations of heavy cycloalkane compounds in the LCF results in elevated low-temperature viscosity and a higher freezing point.[21] On the other hand, the reduced aromatic content in the blend contributes to improved combustion characteristics, including lower soot formation tendency and cleaner burning behavior. Overall, neat LCF exhibits intrinsic limitations, mainly due to imbalances in hydrocarbon distribution, as excessive amounts of light or heavy components can affect the flash point and cold-flow properties, and to a deficiency in *n*-/iso-alkanes, which are crucial for ignition quality and fuel compatibility. Thus, controlling the carbon atom distribution within the liquid product is vital for achieving aviation-grade performance. Meanwhile, aromatic hydrocarbon-based lignin fuels may serve as alternatives to the aromatic fraction in Jet A. Their Tier α predictions are also shown in Fig. 14, where the performance range of conventional aromatics is shaded in purple.[3,277] Although several properties of these lignin-derived aromatics lie outside ASTM specification limit, they offer advantageous features such as lower surface tension, freezing point, and flash point, along with a higher heat of combustion, suggesting their promise in targeted blending strategies.

Table 5 The desired molecules towards different properties

| Property	Favorable compounds	Ref.
Density and viscosity	Alkylcyclohexane with more than 6 carbons, 1,3-diisopropylcyclohexane, *cis*-decalin	272
Energy density and enthalpy savings	Mono-cycloalkanes containing ring structures with 8, 9, or 10 carbon atoms	271
Derived cetane number (DCN)	Cycloheptane	272
Swelling	*cis*-1,2-Dimethylcyclooctane, *cis*-decalin	279
Soot tendency	*n*-Butylcyclohexane, dimethylcyclooctane	280
Flash point	*n*-Butylcyclohexane	281
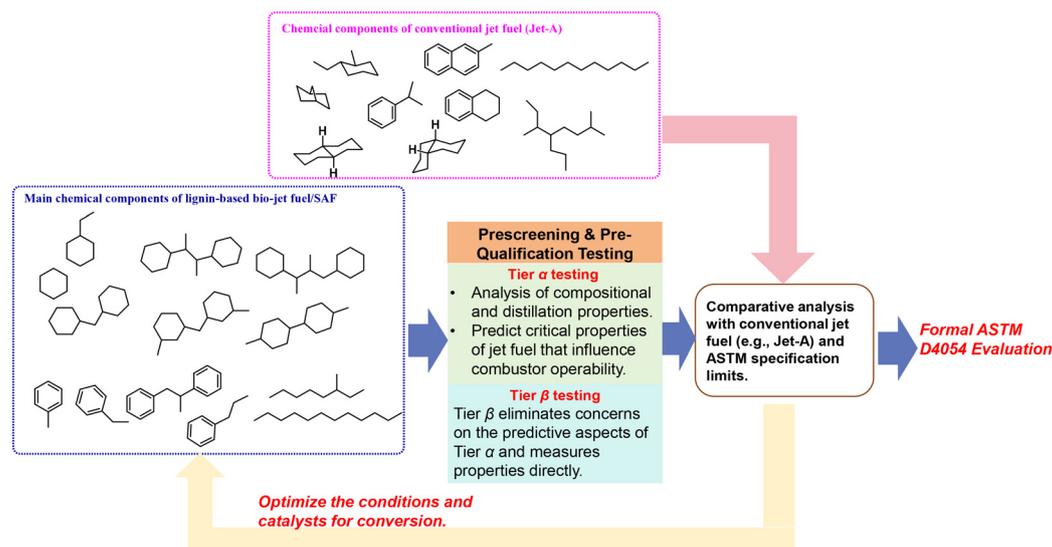
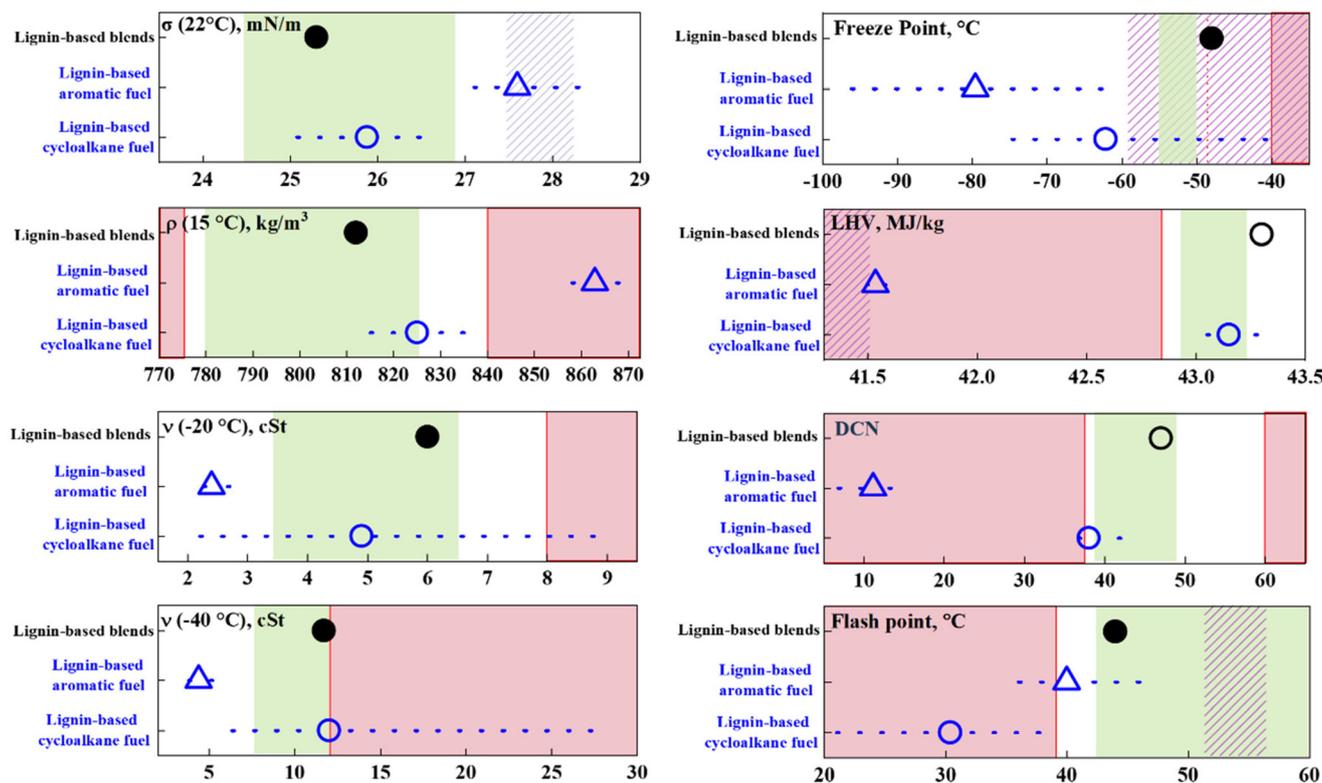**Fig. 13** Profile of evaluation of a novel synthetic SAF by a two-tier prescreening.

Fig. 14 Prescreening of neat lignin-derived cycloalkane fuels (LCF), lignin-derived aromatic fuels, and LCF 10/90 vol% blends with Jet-A, compiled from ref. 3 with permission from Elsevier, copyright 2022; ref. 276 with permission from Elsevier, copyright 2024; and ref. 277 with permission from Elsevier, copyright 2025. Tier α prediction of full distillate of neat LCF and aromatic fuels, Tier β measurement of LCF blended with Jet A, except for DCN and lower heating value (LHV). Dashed lines represent 95% confidence intervals. Red vertical lines denote ASTM specification limits; red-shaded zones highlight out-of-spec regions. Green-shaded areas represent the typical range for conventional Jet-A fuels, while the purple-shaded zones indicate the property range for conventional aromatic fractions in jet fuel.

While conversion pathways undoubtedly influence final fuel characteristics, current data remain insufficient for broad generalizations. Moreover, although feedstock type has long been viewed as a key determinant of fuel quality, recent studies by Stone *et al.* suggest minimal differences between hardwood- and softwood-derived fuels, supporting the flexible use of mixed feedstocks to accommodate seasonal variation.[277]

5. Life-cycle and techno-economic analysis

A robust assessment of industrial feasibility requires integrating environmental and techno-economic assessments. Given its broad global availability, lignocellulosic biomass is widely regarded as a promising and scalable feedstock for SAF production.[282,283] Moriarty *et al.*[13] quantified that woody biomass availability in U.S. port regions far exceeds that of crop residues and waste oils. Techno-economic assessments further indicate that regional woody biomass enables the lowest minimum fuel selling price (MFSP), typically $0.5–2.5 gallon of gasoline equivalent (GGE)$^{-1}$, achieving cost parity with petroleum jet fuel when the feedstock price

remains below $88 per dry ton. However, the specific capital investment per GGE remains higher than for used cooking oil pathways, reflecting a less mature investment ecosystem for lignocellulosic biorefineries. Conversion technology is one of the key factors determining the overall techno-economic and environmental performance of biomass-to-fuel pathways. As discussed above, reductive "lignin-first" fractionation and RCD, in combination with HDO, appear to be promising pathways for producing structurally compatible cycloalkane SAFs. Yet, comprehensive assessments of the entire process are still limited. Bartling *et al.*[284] reported that a hydrogen-free RCF system exhibited a lower global warming potential (GWP) than methanol-based systems and was slightly higher than ethanol-based ones, due to the additional energy demand for *in situ* hydrogen generation. Hydrogen-free yielded an MSP of $1.34 per kg for RCF oil. However, a high recycling rate for the RCF reaction solvent not only markedly reduces fuel and energy consumption but also diminishes the process's sensitivity to woody residue feedstock prices. These combined effects result in reducing the lowest minimum selling price (MSP) from €2261 per t to below €1000 per t and the GWP from 4.42 to 0.71 kg CO_2 per kg (excluding biogenic carbon uptake), the latter being lower than those of fossil-derived phenol (2.79

and benzene (1.86).[36] For standalone HDO processes targeting cycloalkane production, the overall efficiency is highly dependent on hydrogen consumption. The integration of *in situ* hydrogen generation can effectively mitigate carbon emissions; however, careful consideration must be given to catalyst preparation and the life-cycle impacts of hydrogen donors on the global GWP.[285] Consistent with the conclusions of Bagnato *et al.*,[286] who reported an MFSP of $0.79 per kg and emphasized that HDO-only SAF pathways are only marginally viable without co-product valorization, lignin-to-fuel routes more broadly also suffer from negative or near-zero profit margins, aligning with the techno-economic assessment summarized by Wong *et al.*[283]

The deep integration of lignin valorization with pulp and paper mills enables the utilization of existing infrastructure and centralized energy systems to upgrade black liquor into cycloalkanes for SAF.[287] Weyand *et al.*[288] demonstrated that integrating black liquor upgrading within pulp mills achieves a 72–89% GWP reduction depending on the allocation method, surpassing the EU RED II limit (65%), at €1.66 per L, which could reach market parity under carbon prices of around €500 per t CO_2-eq. Similar synergistic benefits were analyzed by Witthayolankowit *et al.*,[289] who evaluated an integrated concept coupling cellulose-to-Lyocell conversion with lignin-to-SAF upgrading from beetle-infested spruce, which offered clear environmental advantages over conventional cotton fiber production. Similarly, Qian *et al.*[290] investigated an integrated biorefinery that combines the poplar-based RCF-HDO pathway with pyrolysis of carbohydrate residues. The integration significantly enhances system-wide carbon utilization, resulting in substantial environmental benefits. The life-cycle assessment indicated that the overall GHG emissions are 44–79% lower than those of fossil-based fuel pathways, while the composite environmental impact index is significantly lower than that of conventional lignocellulosic ethanol routes. The process achieved an MFSP of approximately $1065 per t, and the co-production of high-value furan compounds provided by-product credits that reduce the MFSP of the cycloalkane fuel by 20–30%, thereby improving both the economic viability and the environmental performance of the integrated configuration. Klein *et al.*[291] conducted a multi-criteria optimization that jointly considers economic, environmental, and market/commercial factors to identify the most competitive configuration of lignocellulosic valorization. Poplar-based biorefineries generally outperform those utilizing corn stover, primarily due to their higher carbon efficiency and more favorable process integration. In an integrated configuration coupling cellulose-derived ethanol production with lignin valorization, the catalytic conversion of lignin to cycloalkanes markedly improved carbon utilization, achieving 52.5% for poplar compared with 37% for lignin combustion. However, this pathway exhibited a slightly higher GWP due to the use of fossil-derived methanol as the reaction solvent. Economically, the optimized poplar system achieved a threshold internal rate of return (IRR) of approximately 10%, as reported from Klein *et al.*[291] Considering that D3 Renewable

Identification Number (RIN) credit prices historically exceeded $0.80 per gal for nearly 88% of the observed period, this result suggests that the poplar-based route could be commercially viable under realistic market conditions.

The flexibility of the integrated biorefinery framework for SAF production is manifested in its enhanced resource efficiency, which significantly lowers process fuel and energy consumption. The integrated utilization of woody biomass enables the amortization of feedstock costs *via* high-value co-products, while the use of waste lignin as an internal feedstock stream further reduces exposure to feedstock price volatility. The conversion pathways like RCF/RCD-HDO are encouraged for SAF production in this review. These processes are inherently hydrogen-intensive. The adoption of green hydrogen, combined with ongoing advances in process energy efficiency, is therefore critical to achieving substantial lifecycle emission reductions. Further progress is also needed to address key engineering challenges, including enhancing catalyst stability and optimizing wastewater treatment, to ensure long-term commercial viability.

6. Conclusions and outlook

Lignin, with its rich aromatic structure, particularly from hardwood sources, holds great potential as a feedstock for producing "drop-in" SAFs. Through the extraction of bio-oil from lignin or lignocellulose followed by HDO, lignin-derived hydrocarbons can be obtained with molecular features and oxygen contents close to those required for aviation fuels.

(1) "Lignin-first" biorefining of lignocellulose effectively produces high-quality bio-oil with favorable element ratios and M_w values. Inherent functional groups in lignocellulose can act as an internal hydrogen source, highlighting its potential for decarbonization. HTL of lignin can break interunit C–C linkages in an inert atmosphere over zeolites, while pyrolysis and catalytic depolymerization yield higher quantities of phenolic monomer and dimers. RCD, operating at lower temperatures with reduced reliance on hydrogen and alcohol, shows promising potential for large-scale applications.

(2) Factors such as the surface electron environment, defects, geometric arrangement of reactants on the catalyst surface, and distances between metals and acidic sites collectively influence product selectivity during HDO. Generally, increasing the Brønsted/Lewis acid ratio promotes cycloalkane production, while enhancing Lewis acid/oxophilic sites facilitates the formation of arenes. Larger metal particles foster the HYD pathway, whereas smaller particles favor the direct DDO pathway. Medium to strong oxophilic metals combined with highly active hydrogenation metals enhance cycloalkane production, whereas strong oxophilic metals paired with less active hydrogenation metals promote aromatics formation.

(3) HDO conditions are generally harsh, relying on external hydrogen sources and high energy input. Although some reports have suggested that hydrogen donors or buffers can alleviate the severity of the HDO of phenolic compounds, this

remains a challenge, especially when aiming for realistic oil under mild conditions.

(4) Synthesizing 100% SAF poses greater challenges than blending fossil jet fuel components. Hydrocarbons derived from lignin share similarities in molecular composition with conventional aviation fuels, indicating potential to meet jet fuel performance and operational standards. Preliminary pre-screening data suggest that certain properties of neat lignin-derived cycloalkane fuels may be suboptimal, particularly in terms of flash point, low-temperature viscosity, and DCN. These limitations highlight the need for further fractionation to remove undesirable components that negatively impact performance.

(5) Lignin-to-cycloalkane SAF routes can deliver GHG reductions and competitive economics when integrated with broader biorefinery systems and supported by co-product valorization. Future improvements in hydrogen management, solvent cycles, and reactor-catalyst integration will further enhance carbon efficiency and industrial scalability.

The molecular formulation of bio-oil defines the basic carbon skeleton of liquid fuel. Consequently, evaluating lignin-derived oil extends beyond measuring monomer yield, M_w, and elemental distribution. A thorough molecular formulation of evaluation, covering composition, ratios, and structural characteristics, is necessary. Several studies have suggested specific molecules desirable for jet fuel, emphasizing the importance of future catalytic conversion processes that selectively target beneficial molecules. Alternatively, additional upgrading processes such as alkylation and dimerization may become necessary, presenting new challenges for industrialization and decarbonization efforts. While numerous studies have explored the potential of novel catalysts in producing aviation fuels by refining bio-oils, the majority have predominantly concentrated on characterizing hydrocarbons, with limited reports on conducting α and β tier prescreening. Indeed, a disparity exists between synthetic hydrocarbons and "drop-in" aviation fuel. Conducting two-tier prescreening to evaluate the suitability of hydrocarbons in aviation engines is critical. Moreover, the results from prescreening tests offer essential insights into formulating 100% sustainable aviation fuels at a molecular level.

Conflicts of interest

The authors declare that they have no known competing financial interests or personal relationships that could have appeared to influence the work reported in this paper.

Data availability

No primary research results, software or code have been included and no new data were generated or analysed as part of this review.

Acknowledgements

References

1 P. Hirunsit, A. Senocrate, C. E. Gómez-Camacho and F. Kiefer, *ACS Sustainable Chem. Eng.*, 2024, **12**, 12143–12160.

2 L. Martinez-Valencia, S. Peterson, K. Brandt, A. B. King, M. Garcia-Perez and M. Wolcott, *J. Cleaner Prod.*, 2023, **404**, 136934.

3 M. L. Stone, M. S. Webber, W. P. Mounfield, D. C. Bell, E. Christensen, A. R. C. Morais, Y. Li, E. M. Anderson, J. S. Heyne, G. T. Beckham and Y. Román-Leshkov, *Joule*, 2022, **6**, 2324–2337.

4 M. M. Uddin, U. Lee, H. Xu, Y. Li, H. Kwon, Y. Zhang, S. Smolinski, H. Cai and L. Tao, *Appl. Energy*, 2025, **398**, 126373.

5 S. van Dyk, J. Su, J. D. Mcmillan and J. Saddler, *Biofuels, Bioprod. Biorefin.*, 2019, **13**, 760–775.

6 G. Seber, N. Escobar, H. Valin and R. Malina, *Renewable Sustainable Energy Rev.*, 2022, **170**, 112945.

7 A. H. Bhatt, Y. Zhang, A. Milbrandt, E. Newes, K. Moriarty, B. Klein and L. Tao, *Energy Convers. Manage.*, 2023, **275**, 116441.

8 R. S. Capaz, J. A. Posada, P. Osseweijer and J. E. A. Seabra, *Resour., Conserv. Recycl.*, 2021, **166**, 105260.

9 R. S. Capaz, E. Guida, J. E. A. Seabra, P. Osseweijer and J. A. Posada, *Biofuels, Bioprod. Biorefin.*, 2021, **15**, 502–524.

10 Z. Xu, Y. Fan, Y. Zheng, S. Ding, M. Zhu, G. Li, M. Wang, Z. Yu, Y. Song, L. Chang and L. Chen, *Environ. Pollut.*, 2025, **368**, 125661.

11 U.S. Department of Energy, Alternative Aviation Fuels: Overview of Challenges, Opportunities, and Next Steps, DOE/EE-1515, Washington, DC, 2017.

12 J. Popp, S. Kovács, J. Oláh, Z. Divéki and E. Balázs, *New Biotechnol.*, 2021, **60**, 76–84.

13 K. Moriarty, A. Milbrandt and L. Tao, *Port Authority of New York and New Jersey Sustainable Aviation Fuel Logistics and Production Study*, National Renewable Energy Lab. (NREL), Golden, CO, United States, 2021.

14 J. Cárdenas, A. Orjuela, D. L. Sánchez, P. C. Narváez, B. Katryniok and J. Clark, *J. Cleaner Prod.*, 2021, **289**, 125129.

15 P. Yadav, D. Athanassiadis, I. Antonopoulou, U. Rova, P. Christakopoulos, M. Tysklind and L. Matsakas, *J. Cleaner Prod.*, 2021, **279**, 123515.

16 M. S. Webber, J. Watson, J. Zhu, J. H. Jang, M. Çağlayan, J. S. Heyne, G. T. Beckham and Y. Román-Leshkov, *Nat. Mater.*, 2024, **23**, 1622–1638.

17 J. Xu, J. Qiu, L. Zhang and J. Yao, *Appl. Catal., B*, 2025, **361**, 124639.

18 C. Huang, Q. Qin, Y. Liu, G. Duan, P. Xiao, Y. Huang, C. Mei, X. Han, J. Han, S. He and S. Jiang, *Chem. Soc. Rev.*, 2025, **54**, 9027–9091.

19 F. F. Menezes, V. M. Nascimento, G. R. Gomes, G. J. M. Rocha, M. Strauss, T. L. Junqueira and C. Driemeier, *Fuel*, 2023, **342**, 127796.

20 M. Mujtaba, L. F. Fraceto, M. Fazeli, S. Mukherjee, S. M. Savassa, G. Araujo de Medeiros, A. do Espírito Santo Pereira, S. D. Mancini, J. Lipponen and F. Vilaplana, *J. Cleaner Prod.*, 2023, **402**, 136815.

21 Z. Yang, Z. Xu, M. Feng, J. R. Cort, R. Gieleciak, J. Heyne and B. Yang, *Fuel*, 2022, **321**, 124040.

22 X. Lv, C. Zhao, N. Yan, X. Ma, S. Feng and L. Shuai, *Bioresour. Technol.*, 2025, **419**, 132039.

23 F. Cheng and C. E. Brewer, *Renewable Sustainable Energy Rev.*, 2017, **72**, 673–722.

24 S. Dooley, J. Heyne, S. H. Won, P. Dievart, Y. Ju and F. L. Dryer, *Energy Fuels*, 2014, **28**, 7649–7661.

25 J. Holladay, Z. Abdullah and J. Heyne, *Sustainable Aviation Fuel: Review of Technical Pathways*, U.S. Department of Energy, Bioenergy Technologies Office (BETO), Washington, DC, 2020.

26 D. Carpenter, S. Nates, F. L. Dryer and S. H. Won, *Combust. Flame*, 2021, **223**, 243–253.

27 J. Su, S. van Dyk and J. Saddler, *J. Cleaner Prod.*, 2022, **376**, 134335.

28 B. H. H. Goh, C. T. Chong, H. C. Ong, T. Seljak, T. Katrašnik, V. Józsa, J.-H. Ng, B. Tian, S. Karmarkar and V. Ashokkumar, *Energy Convers. Manage.*, 2022, **251**, 114974.

29 C. A. Scaldaferri and V. M. D. Pasa, *Fuel*, 2019, **245**, 458–466.

30 Z. Yu, W. Kong, W. Liang, Y. Guo, J. Cui, Y. Hu, Z. Sun, S. Elangovan and F. Xu, *ChemSusChem*, 2025, **18**, e202401399.

31 S. Shao, X. Wang, W. Li, Y. Zhang, S. Liu, W. Xiao, Z. Yue, X. Lu and X. Fan, *Catal. Sci. Technol.*, 2025, **15**, 962–987.

32 M. V. Galkin and J. S. M. Samec, *ChemSusChem*, 2016, **9**, 1544–1558.

33 M. Zhang, Y. Hu, H. Wang, H. Li, X. Han, Y. Zeng and C. C. Xu, *Mol. Catal.*, 2021, **504**, 111438.

34 M. Saidi, F. Samimi, D. Karimipourfard, T. Nimmanwudipong, B. C. Gates and M. R. Rahimpour, *Energy Environ. Sci.*, 2014, **7**, 103–129.

35 P. He, L. Li, Y. Shao, Q. Yi, Z. Liu, H. Geng, Y. Liu and V. Valtchev, *ChemCatChem*, 2024, **16**, e202301681.

36 W. Arts, K. Van Aelst, E. Cooreman, J. Van Aelst, S. Van den Bosch and B. F. Sels, *Energy Environ. Sci.*, 2023, **16**, 2518–2539.

37 A. Kumar, M. Jindal, S. Maharana and B. Thallada, *Energy Fuels*, 2021, **35**, 16965–16994.

38 T. Renders, S. Van den Bosch, S. F. Koelewijn, W. Schutyser and B. F. Sels, *Energy Environ. Sci.*, 2017, **10**, 1551–1557.

39 M. M. Abu-Omar, K. Barta, G. T. Beckham, J. S. Luterbacher, J. Ralph, R. Rinaldi, Y. Román-Leshkov,

J. S. M. Samec, B. F. Sels and F. Wang, *Energy Environ. Sci.*, 2021, **14**, 262–292.

40 X. Li, Y. Xu, K. Alorku, J. Wang and L. Ma, *Mol. Catal.*, 2023, **550**, 113551.

41 M. Jindal, P. Uniyal and B. Thallada, *Bioresour. Technol.*, 2023, **385**, 129396.

42 Z. Liu, H. Li, X. Gao, X. Guo, S. Wang, Y. Fang and G. Song, *Nat. Commun.*, 2022, **13**, 4716.

43 Q. Song, F. Wang and J. Xu, *Chem. Commun.*, 2012, **48**, 7019–7021.

44 D. J. van de Pas and K. M. Torr, *Biomacromolecules*, 2017, **18**, 2640–2648.

45 S. Van den Bosch, T. Renders, S. Kennis, S. F. Koelewijn, G. Van den Bossche, T. Vangeel, A. Deneyer, D. Depuydt, C. M. Courtin, J. M. Thevelein, W. Schutyser and B. F. Sels, *Green Chem.*, 2017, **19**, 3313–3326.

46 F. Brienza, K. Van Aelst, F. Devred, D. Magnin, B. F. Sels, P. Gerin, I. Cybulska and D. P. Debecker, *ChemSusChem*, 2023, **16**, e202300103.

47 J. Park, H. S. Cahyadi, U. Mushtaq, D. Verma, D. Han, K.-W. Nam, S. K. Kwak and J. Kim, *ACS Catal.*, 2020, **10**, 12487–12506.

48 Y. Li, Y. Yu, Y. Lou, S. Zeng, Y. Sun, Y. Liu and H. Yu, *Angew. Chem., Int. Ed.*, 2023, **62**, e202307116.

49 T. Renders, G. Van den Bossche, T. Vangeel, K. Van Aelst and B. Sels, *Curr. Opin. Biotechnol.*, 2019, **56**, 193–201.

50 S. Van den Bosch, W. Schutyser, R. Vanholme, T. Driessen, S. F. Koelewijn, T. Renders, B. De Meester, W. J. J. Huijgen, W. Dehaen, C. M. Courtin, B. Lagrain, W. Boerjan and B. F. Sels, *Energy Environ. Sci.*, 2015, **8**, 1748–1763.

51 T. I. Korányi, B. Fridrich, A. Pineda and K. Barta, *Molecules*, 2020, **25**, 2815.

52 E. M. Anderson, M. L. Stone, R. Katahira, M. Reed, G. T. Beckham and Y. Román-Leshkov, *Joule*, 2017, **1**, 613–622.

53 W. Schutyser, S. Van den Bosch, T. Renders, T. De Boe, S. F. Koelewijn, A. Dewaele, T. Ennaert, O. Verkinderen, B. Goderis, C. M. Courtin and B. F. Sels, *Green Chem.*, 2015, **17**, 5035–5045.

54 T. Renders, W. Schutyser, S. Van den Bosch, S.-F. Koelewijn, T. Vangeel, C. M. Courtin and B. F. Sels, *ACS Catal.*, 2016, **6**, 2055–2066.

55 H. D. Thi, K. Van Aelst, S. Van den Bosch, R. Katahira, G. T. Beckham, B. F. Sels and K. M. Van Geem, *Green Chem.*, 2022, **24**, 191–206.

56 Z. Cao, M. Dierks, M. T. Clough, I. B. Daltro de Castro and R. Rinaldi, *Joule*, 2018, **2**, 1118–1133.

57 G. G. Facas, D. G. Brandner, J. R. Bussard, Y. Román-Leshkov and G. T. Beckham, *ACS Sustainable Chem. Eng.*, 2023, **11**, 4517–4522.

58 Y. Liu, N. Deak, Z. Wang, H. Yu, L. Hameleers, E. Jurak, P. J. Deuss and K. Barta, *Nat. Commun.*, 2021, **12**, 5424.

59 Y. Yu, W. Cheng, Y. Li, T. Wang, Q. Xia, Y. Liu and H. Yu, *Green Chem.*, 2022, **24**, 3257–3268.

60 V. Sharma, M.-L. Tsai, C.-W. Chen, P.-P. Sun, A. K. Patel, R. R. Singhania, P. Nargotra and C.-D. Dong, *Bioresour. Technol.*, 2022, **360**, 127631.

61 M. V. Galkin, A. T. Smit, E. Subbotina, K. A. Artemenko, J. Bergquist, W. J. J. Huijgen and J. S. M. Samec, *ChemSusChem*, 2016, **9**, 3280–3287.

62 H. Zhou, X. Liu, Y. Guo and Y. Wang, *JACS Au*, 2023, **3**, 1911–1917.

63 D. Li, Y. Li, X. Liu, Y. Guo, C.-W. Pao, J.-L. Chen, Y. Hu and Y. Wang, *ACS Catal.*, 2019, **9**, 9671–9682.

64 Y. Zhu, Y. Liao, W. Lv, J. Liu, X. Song, L. Chen, C. Wang, B. F. Sels and L. Ma, *ACS Sustainable Chem. Eng.*, 2020, **8**, 2361–2374.

65 Y. Zhu, Y. Liao, L. Lu, W. Lv, J. Liu, X. Song, J. Wu, L. Li, C. Wang, L. Ma and B. F. Sels, *ACS Catal.*, 2023, **13**, 7929–7941.

66 J. S. Kruger, R. J. Dreiling, D. G. Wilcox, A. J. Ringsby, K. L. Noon, C. K. Amador, D. G. Brandner, K. J. Ramirez, S. J. Haugen, B. C. Klein, R. Davis, R. J. Hanes, R. M. Happs, N. S. Cleveland, E. D. Christensen, J. Miscall and G. T. Beckham, *Green Chem.*, 2022, **24**, 8733–8741.

67 X. Du, A. W. Tricker, W. Yang, R. Katahira, W. Liu, T. T. Kwok, P. Gogoi and Y. Deng, *ACS Sustainable Chem. Eng.*, 2021, **9**, 7719–7727.

68 H. Luo, E. P. Weeda, M. Alherech, C. W. Anson, S. D. Karlen, Y. Cui, C. E. Foster and S. S. Stahl, *J. Am. Chem. Soc.*, 2021, **143**, 15462–15470.

69 R. Patel, P. Dhar, A. Babaei-Ghazvini, M. N. Dafchahi and B. Acharya, *Bioresour. Technol. Rep.*, 2023, **22**, 101463.

70 R. Rinaldi, R. Jastrzebski, M. T. Clough, J. Ralph, M. Kennema, P. C. A. Bruijnincx and B. M. Weckhuysen, *Angew. Chem., Int. Ed.*, 2016, **55**, 8164–8215.

71 S. Cademartori, Lignin: Building Block of a Low-Carbon Economy, in *Pulp & Paper Canada*, Spring, 2020.

72 J. S. Gregg, S. Bolwig, T. Hansen, O. Solér, S. B. Amer-Allam, J. P. Viladecans, A. Klitkou and A. Fevolden, *Sustainability*, 2017, **9**, 118.

73 T. Phongpreecha, N. C. Hool, R. J. Stoklosa, A. S. Klett, C. E. Foster, A. Bhalla, D. Holmes, M. C. Thies and D. B. Hodge, *Green Chem.*, 2017, **19**, 5131–5143.

74 S. Wang, X. Li, R. Ma and G. Song, *Acc. Chem. Res.*, 2025, **58**, 529–542.

75 X. Liu, F. P. Bouxin, J. Fan, V. L. Budarin, C. Hu and J. H. Clark, *ChemSusChem*, 2020, **13**, 4296–4317.

76 E. Leng, Y. Guo, J. Chen, S. Liu, J. E and Y. Xue, *Fuel*, 2022, **309**, 122102.

77 S. Zhou, Y. Xue, A. Sharma and X. Bai, *ACS Sustainable Chem. Eng.*, 2016, **4**, 6608–6617.

78 J. Yu, D. Wang and L. Sun, *Fuel*, 2021, **290**, 120078.

79 D. Chen, K. Cen, X. Zhuang, Z. Gan, J. Zhou, Y. Zhang and H. Zhang, *Combust. Flame*, 2022, **242**, 112142.

80 Q. Lu, W.-L. Xie, B. Hu, J. Liu, W. Zhao, B. Zhang and T.-P. Wang, *Combust. Flame*, 2021, **225**, 395–405.

81 D. Cui, H. Yin, S. Pan, S. Wu, J. Li, Y. Liu and Q. Wang, *J. Energy Inst.*, 2023, **109**, 101262.

82 Y. S. Choi, R. Singh, J. Zhang, G. Balasubramanian, M. R. Sturgeon, R. Katahira, G. Chupka, G. T. Beckham and B. H. Shanks, *Green Chem.*, 2016, **18**, 1762–1773.

83 L. Wang, J. Yin, J. Jiang, Y. Zhang, M. Song, R. Zhang, Z. Dong, H. Yang and H. Yu, *Fuel*, 2022, **317**, 123531.

84 M. Lei, S. Wu, C. Liu, J. Liang and R. Xiao, *Fuel Process. Technol.*, 2021, **217**, 106812.

85 H. Ma, T. Li, S. Wu and X. Zhang, *Bioresour. Technol.*, 2020, **309**, 123351.

86 H. Yang, Z. Dong, B. Liu, Y. Chen, M. Gong, S. Li and H. Chen, *Fuel*, 2021, **288**, 119719.

87 T. Li, H. Ma, S. Wu and Y. Yin, *Energy Convers. Manage.*, 2020, **207**, 112551.

88 P. F. Britt, M. K. Kidder and A. C. Buchanan III, *Energy Fuels*, 2007, **21**, 3102–3108.

89 X. Chen, Q. Che, S. Li, Z. Liu, H. Yang, Y. Chen, X. Wang, J. Shao and H. Chen, *Fuel Process. Technol.*, 2019, **196**, 106180.

90 X. Li, F. Yu, X. Chen and Y. Nie, *Fuel*, 2025, **401**, 135946.

91 K. Iisa, R. J. French, K. A. Orton, M. M. Yung, D. K. Johnson, J. ten Dam, M. J. Watson and M. R. Nimlos, *Energy Fuels*, 2016, **30**, 2144–2157.

92 B. Li, L. Ou, Q. Dang, P. Meyer, S. Jones, R. Brown and M. Wright, *Bioresour. Technol.*, 2015, **196**, 49–56.

93 S. Wang, Z. Wan, Y. Han, Y. Jiao, Z. Li, P. Fu, N. Li, A. Zhang and W. Yi, *J. Environ. Chem. Eng.*, 2023, **11**, 109113.

94 A. G. Margellou, P. A. Lazaridis, I. D. Charisteidis, C. K. Nitsos, C. P. Pappa, A. P. Fotopoulos, S. Van den Bosch, B. F. Sels and K. S. Triantafyllidis, *Appl. Catal., A*, 2021, **623**, 118298.

95 Z. Pan, A. Puente-Urbina, S. R. Batool, A. Bodi, X. Wu, Z. Zhang, J. A. van Bokhoven and P. Hemberger, *Nat. Commun.*, 2023, **14**, 4512.

96 D. C. Elliott, P. Biller, A. B. Ross, A. J. Schmidt and S. B. Jones, *Bioresour. Technol.*, 2015, **178**, 147–156.

97 C. Penke, L. Moser and V. Batteiger, *Biomass Bioenergy*, 2021, **151**, 106123.

98 R. Katakojwala, H. Kopperi, S. Kumar and S. V. Mohan, *Bioresour. Technol.*, 2020, **310**, 123369.

99 M. Elhassan, R. Abdullah, M. R. R. Kooh and Y.-F. Chou Chau, *Bioresour. Technol. Rep.*, 2023, **21**, 101314.

100 P. Yadav and S. N. Reddy, *Ind. Crops Prod.*, 2023, **198**, 116677.

101 S. S. Toor, L. Rosendahl and A. Rudolf, *Energy*, 2011, **36**, 2328–2342.

102 L. Nazari, Z. Yuan, S. Souzanchi, M. B. Ray and C. Xu, *Fuel*, 2015, **162**, 74–83.

103 M. Y. Lui, B. Chan, A. K. L. Yuen, A. F. Masters and T. Maschmeyer, *ChemSusChem*, 2020, **13**, 2002–2006.

104 M. Otromke, R. J. White and J. Sauer, *Carbon Resour. Convers.*, 2019, **2**, 59–71.

105 M. Y. Lui, B. Chan, A. K. L. Yuen, A. F. Masters, A. Montoya and T. Maschmeyer, *ChemSusChem*, 2017, **10**, 2140–2144.

106 B. Ciuffi, M. Loppi, A. M. Rizzo, D. Chiaramonti and L. Rosi, *Sci. Rep.*, 2021, **11**, 15504.

107 W.-J. Liu and H.-Q. Yu, *ACS Environ. Au*, 2022, **2**, 98–114.

108 S. Sobek, Q. K. Tran, R. Junga, M. Sajdak and S. Werle, *Biomass Bioenergy*, 2023, **172**, 106768.

109 M. Scarsella, B. de Caprariis, M. Damizia and P. De Filippis, *Biomass Bioenergy*, 2020, **140**, 105662.

110 J. Yan, Q. Meng, X. Shen, B. Chen, Y. Sun, J. Xiang, H. Liu and B. Han, *Sci. Adv.*, 2020, **6**, eabd1951.

111 X. Kong, C. Liu, Y. Fan, M. Li and R. Xiao, *ACS Catal.*, 2023, **13**, 10048–10055.

112 X. Lu, L. Lagerquist, K. Eränen, J. Hemming, P. Eklund, L. Estel, S. Leveneur and H. Grénman, *Ind. Eng. Chem. Res.*, 2021, **60**, 16827–16838.

113 D. V. Sahayaraj, A. Lusi, E. M. Mitchell, X. Bai and J.-P. Tessonnier, *Green Chem.*, 2021, **23**, 7731–7742.

114 D. V. Sahayaraj, A. Lusi, A. J. Kohler, H. Bateni, H. Radhakrishnan, A. Saraeian, B. H. Shanks, X. Bai and J.-P. Tessonnier, *Energy Environ. Sci.*, 2023, **16**, 97–112.

115 L. Feng, X. Li, Z. Wang and B. Liu, *Bioresour. Technol.*, 2021, **323**, 124569.

116 M. S. Kollman, X. Jiang, R. Sun, X. Zhang, W. Li, H.-M. Chang and H. Jameel, *Chem. Eng. J.*, 2023, **451**, 138464.

117 C. Zhang, J. Lu, X. Zhang, K. MacArthur, M. Heggen, H. Li and F. Wang, *Green Chem.*, 2016, **18**, 6545–6555.

118 B. Luo, Z. Tian, R. Shu, C. Wang, Y. Chen, J. Liu and Y. Liao, *J. Catal.*, 2025, **442**, 115914.

119 J. Wang, S. Hong, B. Wang, X. Shen, J.-L. Wen and T.-Q. Yuan, *Chem. Catal.*, 2023, **3**, 100797.

120 L. Shuai, J. Sitison, S. Sadula, J. Ding, M. C. Thies and B. Saha, *ACS Catal.*, 2018, **8**, 6507–6512.

121 Y. Shao, Q. Xia, L. Dong, X. Liu, X. Han, S. F. Parker, Y. Cheng, L. L. Daemen, A. J. Ramirez-Cuesta, S. Yang and Y. Wang, *Nat. Commun.*, 2017, **8**, 16104.

122 X. Kong, C. Liu, H. Zeng, Y. Fan, H. Zhang and R. Xiao, *ChemSusChem*, 2024, **17**, e202300996.

123 R. Lou, G. Lyu, S. Wu, B. Zhang, H. Zhao and L. A. Lucia, *ACS Sustainable Chem. Eng.*, 2018, **6**, 430–437.

124 L. Dong, L. Lin, X. Han, X. Si, X. Liu, Y. Guo, F. Lu, S. Rudić, S. F. Parker, S. Yang and Y. Wang, *Chem*, 2019, **5**, 1521–1536.

125 H. Zhou, L. Chen, Y. Guo, X. Liu, X.-P. Wu, X.-Q. Gong and Y. Wang, *ACS Catal.*, 2022, **12**, 4806–4812.

126 B. M. Matsagar, Z.-Y. Wang, C. Sakdaronnarong, S. S. Chen, D. C. W. Tsang and K. C.-W. Wu, *ChemCatChem*, 2019, **11**, 4604–4616.

127 J. Wang, X. Yao, Y. Li, J. Zhang, C. Zhao and T. J. Strathmann, *ACS Omega*, 2023, **8**, 19969–19975.

128 L. Li, L. Dong, D. Li, Y. Guo, X. Liu and Y. Wang, *ACS Catal.*, 2020, **10**, 15197–15206.

129 J.-W. Zhang, G.-P. Lu and C. Cai, *Green Chem.*, 2017, **19**, 4538–4543.

130 Z. Dou, Z. Zhang and M. Wang, *Appl. Catal., B*, 2022, **301**, 120767.

131 Y. Hu, L. Yan, X. Zhao, C. Wang, S. Li, X. Zhang, L. Ma and Q. Zhang, *Green Chem.*, 2021, **23**, 7030–7040.

132 M. Peng, M. Shen, T. Muraishi, X. Wei, L. Fan, T. Tsunakawa, K. Kamiya and E. W. Qian, *Fuel*, 2023, **354**, 129369.

133 Y. Zhang, S. Jia, X. Wang, H. Deng, W. Xu and J. Shi, *Int. J. Biol. Macromol.*, 2023, **253**, 127363.

134 Y. Zhang, W. Xu, H. Deng, D. Zhang, X. Li and J. Shi, *Ind. Crops Prod.*, 2023, **205**, 117481.

135 W. Deng, H. Zhang, X. Wu, R. Li, Q. Zhang and Y. Wang, *Green Chem.*, 2015, **17**, 5009–5018.

136 K. R. Alunga, Y.-Y. Ye, S-R. Li, D. Wang and Y.-Q. Liu, *Catal. Sci. Technol.*, 2015, **5**, 3746–3753.

137 X. Wang, Y. Zhang, S. Jia, H. Deng, W. Xu and J. Shi, *Ind. Crops Prod.*, 2024, **207**, 117750.

138 C. Liu, S. Wu, H. Zhang and R. Xiao, *Fuel Process. Technol.*, 2019, **191**, 181–201.

139 M. Liu and P. J. Dyson, *Nat. Commun.*, 2023, **14**, 2830.

140 W. Lan, J. B. de Bueren and J. S. Luterbacher, *Angew. Chem., Int. Ed.*, 2019, **58**, 2649–2654.

141 C. Sun, L. Zheng, W. Xu, A. V. Dushkin and W. Su, *Green Chem.*, 2020, **22**, 3489–3494.

142 Y. Cui, S. L. Goes and S. S. Stahl, Sequential oxidation–depolymerization strategies for lignin conversion to low molecular weight aromatic chemicals, in *Advances in Inorganic Chemistry*, ed. P. C. Ford and R. van Eldik, Academic Press, 2021, vol. 77, pp. 99–136.

143 M. Wang, L. H. Li, J. M. Lu, H. J. Li, X. C. Zhang, H. F. Liu, N. C. Luo and F. Wang, *Green Chem.*, 2017, **19**, 702–706.

144 L. Waura-angkura, B. M. Matsagar, K. Lee, V. Pavarajarn and K. C. W. Wu, *Green Chem.*, 2024, **26**, 1889–1900.

145 J. Liang, M.-X. Wang, Y.-P. Zhao, W.-W. Yan, X.-G. Si, G. Yu, J.-P. Cao and X.-Y. Wei, *ChemCatChem*, 2021, **13**, 3836–3845.

146 X. Ren, P. Wang, X. Han, G. Zhang, J. Gu, C. Ding, X. Zheng and F. Cao, *ACS Sustainable Chem. Eng.*, 2017, **5**, 6548–6556.

147 S. van Dyk, J. Su, M. Ebadian, D. O'Connor, M. Lakeman and J. Saddler, *Biotechnol. Biofuels*, 2019, **12**, 281.

148 H. Ramsurn and R. B. Gupta, *Energy Fuels*, 2012, **26**, 2365–2375.

149 M. B. Figueirêdo, I. Hita, P. J. Deuss, R. H. Venderbosch and H. J. Heeres, *Green Chem.*, 2022, **24**, 4680–4702.

150 R. J. M. Westerhof, N. J. M. Kuipers, S. R. A. Kersten and W. P. M. van Swaaij, *Ind. Eng. Chem. Res.*, 2007, **46**, 9238–9247.

151 Z. E. Zadeh, A. Abdulkhani and B. Saha, *Energy*, 2021, **214**, 118930.

152 F. Chireshe, F.-X. Collard and J. F. Görgens, *J. Anal. Appl. Pyrolysis*, 2020, **146**, 104751.

153 H. Paysepar, K. T. V. Rao, Z. Yuan, H. Shui and C. Xu, *J. Anal. Appl. Pyrolysis*, 2020, **149**, 104842.

154 A. do Couto Fraga, M. B. B. de Almeida and E. F. Sousa-Aguiar, *Cellulose*, 2021, **28**, 2003–2020.

155 X. Peng, X. Ma, Y. Lin, J. Wang and X. Chen, *J. Anal. Appl. Pyrolysis*, 2019, **141**, 104621.

156 M. Shahabuddin, E. Italiani, A. R. Teixeira, N. Kazantzis and M. T. Timko, *ACS Sustainable Chem. Eng.*, 2023, **11**, 733–743.

157 H. Yang, R. Coolman, P. Karanjkar, H. Wang, P. Dornath, H. Chen, W. Fan, W. C. Conner, T. J. Mountziaris and G. Huber, *Green Chem.*, 2017, **19**, 286–297.

158 H. Shafaghat, P. S. Rezaei, D. Ro, J. Jae, B.-S. Kim, S.-C. Jung, B. H. Sung and Y.-K. Park, *J. Ind. Eng. Chem.*, 2017, **54**, 447–453.

159 T. N. Trinh, P. A. Jensen, K. Dam-Johansen, N. O. Knudsen, H. R. Sørensen and S. Hvilsted, *Energy Fuels*, 2013, **27**, 1399–1409.

160 K. G. Kalogiannis, L. Matsakas, A. A. Lappas, U. Rova and P. Christakopoulos, *Energies*, 2019, **12**, 1606.

161 M. Sakhakarmy, A. Kemp, B. Biswas, S. Kafle and S. Adhikari, *Energies*, 2024, **17**, 2800.

162 H. Paysepar, K. T. V. Rao, Z. Yuan, L. Nazari, H. Shui and C. Xu, *Fuel Process. Technol.*, 2018, **178**, 362–370.

163 M. Tymchyshyn, A. Rezayan, Z. Yuan, Y. Zhang and C. C. Xu, *Ind. Eng. Chem. Res.*, 2020, **59**, 17239–17249.

164 A. Achour, D. Bernin, D. Creaser and L. Olsson, *Chem. Eng. J.*, 2023, **453**, 139829.

165 J. H. Jang, A. R. C. Morais, M. Browning, D. G. Brandner, J. K. Kenny, L. M. Stanley, R. M. Happs, A. S. Kovvali, J. I. Cutler, Y. Román-Leshkov, J. R. Bielenberg and G. T. Beckham, *Green Chem.*, 2023, **25**, 3660–3670.

166 H. Choi, M. Alherech, J. H. Jang, S. P. Woodworth, K. J. Ramirez, E. M. Karp and G. T. Beckham, *Green Chem.*, 2024, **26**, 5900–5913.

167 Y. Cao, J. Gao, C. Zhang, D. C. W. Tsang, J. Fan, J. H. Clark, G. Luo, X. Zhu and S. Zhang, *ACS Sustainable Chem. Eng.*, 2022, **10**, 15273–15283.

168 Y. Zhu, N. Li, H. Liu, C. Cai, Y. Wang, J. Mu and F. Wang, *ACS Catal.*, 2024, **14**, 16872–16884.

169 P. Lian, S. Liu, Z. Ma, X. Wang and Y. Han, *Ind. Crops Prod.*, 2024, **212**, 118376.

170 C. A. Teles, P. M. de Souza, R. C. Rabelo-Neto, A. Teran, G. Jacobs, D. E. Resasco and F. B. Noronha, *ACS Sustainable Chem. Eng.*, 2021, **9**, 12870–12884.

171 T. Cordero-Lanzac, R. Palos, I. Hita, J. M. Arandes, J. Rodríguez-Mirasol, T. Cordero, J. Bilbao and P. Castaño, *Appl. Catal., B*, 2018, **239**, 513–524.

172 F. Gan, X. Jiang, Z. Jin, M. Tan, X. Xie, Q. Peng, G. Cao and S. Ma, *ACS Catal.*, 2024, **14**, 13324–13333.

173 C. Li, Y. Nakagawa, M. Yabushita, A. Nakayama and K. Tomishige, *ACS Catal.*, 2021, **11**, 12794–12814.

174 Q. Xu, L.-P. Xiao, Q. Wang, L.-L. Zhang and R.-C. Sun, *J. Catal.*, 2024, **435**, 115552.

175 H. Zhang, Q. Wang, X.-Q. Si, H.-Z. Dou, W.-F. Ren, L.-P. Xiao and R.-C. Sun, *ACS Sustainable Chem. Eng.*, 2025, **13**, 6528–6537.

176 X. Yang, J. Yu, M. Zeng, Z. Luo and H. Zhang, *J. Anal. Appl. Pyrolysis*, 2025, **188**, 107049.

177 X. Liu, S. Feng, Q. Fang, Z. Jiang and C. Hu, *Mol. Catal.*, 2020, **495**, 111164.

178 S. Yu, Z. Ge, H. Huang, J. A. Steele, F. Kemausuor, E. M. Hafez, O. Tursunov and Z. Luo, *Chem. Eng. J.*, 2025, **518**, 164669.

179 E. Bartolomei, Y. L. Brech, R. Gadiou, F. Bertaud, S. Leclerc, L. Vidal, J.-M. L. Meins and A. Dufour, *Energy Fuels*, 2021, **35**, 17769–17783.

180 T. Belkheiri, C. Mattsson, S.-I. Andersson, L. Olausson, L.-E. Åmand, H. Theliander and L. Vamling, *Energy Fuels*, 2016, **30**, 4916–4924.

181 Y. Zhu, W. Song, R. Yao, Y. Zhao and G. Xu, *J. Energy Inst.*, 2022, **101**, 187–193.

182 Z. Zhu, L. Rosendahl, S. S. Toor, D. Yu and G. Chen, *Appl. Energy*, 2015, **137**, 183–192.

183 A. P. Pinheiro Pires, M. Garcia-Perez, M. V. Olarte, W. Kew, A. Schmidt, K. Zemaitis, M. Denson, E. Terrell, A. McDonald and Y. Han, *Energy Fuels*, 2023, **37**, 7221–7236.

184 J. M. Jarvis, J. M. Billing, R. T. Hallen, A. J. Schmidt and T. M. Schaub, *Energy Fuels*, 2017, **31**, 2896–2906.

185 Z. Xiong, J. Guo, W. Chaiwat, W. Deng, X. Hu, H. Han, Y. Chen, K. Xu, S. Su, S. Hu, Y. Wang and J. Xiang, *Fuel Process. Technol.*, 2020, **199**, 106299.

186 V. Paasikallio, C. Lindfors, E. Kuoppala, Y. Solantausta, A. Oasmaa, J. Lehto and J. Lehtonen, *Green Chem.*, 2014, **16**, 3549–3559.

187 D. K. Ratnasari, A. Bijl, W. Yang and P. G. Jönsson, *Catalysts*, 2020, **10**, 868.

188 S. Agarwal, R. K. Chowdari, I. Hita and H. J. Heeres, *ACS Sustainable Chem. Eng.*, 2017, **5**, 2668–2678.

189 M. M. Rahman and T. Reza, *Energies*, 2025, **18**, 4773.

190 M. Chen, W. Dai, Y. Wang, Z. Tang, H. Li, C. Li, Z. Yang and J. Wang, *Fuel*, 2023, **333**, 126365.

191 A. R. K. Gollakota, M. Reddy, M. D. Subramanyam and N. Kishore, *Renewable Sustainable Energy Rev.*, 2016, **58**, 1543–1568.

192 M. S. Talmadge, R. M. Baldwin, M. J. Biddy, R. L. McCormick, G. T. Beckham, G. A. Ferguson, S. Czernik, K. A. Magrini-Bair, T. D. Foust, P. D. Metelski, C. Hetrick and M. R. Nimlos, *Green Chem.*, 2014, **16**, 407–453.

193 V. S. Prabhudesai, L. Gurrala and R. Vinu, *Energy Fuels*, 2022, **36**, 1155–1188.

194 X. Wang, Z. Zhang, Z. Yan, Q. Li and Y. Zhang, *Appl. Catal., A*, 2023, **662**, 119266.

195 Z. Yang, B. Luo, R. Shu, Z. Zhong, Z. Tian, C. Wang and Y. Chen, *Fuel*, 2022, **319**, 123617.

196 M. A. Salam, P. Arora, H. Ojagh, Y. W. Cheah, L. Olsson and D. Creaser, *Sustainable Energy Fuels*, 2020, **4**, 149–163.

197 W. Lv, X. Hu, Y. Zhu, Y. Xu, S. Liu, P. Chen, C. Wang and L. Ma, *Renewable Energy*, 2022, **188**, 195–210.

198 X. Zhang, H. Yan, L. Zhu, T. Li and S. Wang, *Adv. Sustainable Syst.*, 2020, **4**, 1900136.

199 X. Zhang, J. Tang, Q. Zhang, Q. Liu, Y. Li, L. Chen, C. Wang and L. Ma, *Catal. Today*, 2019, **319**, 41–47.

200 X. Wang, M. Arai, Q. Wu, C. Zhang and F. Zhao, *Green Chem.*, 2020, **22**, 8140–8168.

201 A. R. K. Gollakota, C.-M. Shu, P. K. Sarangi, K. P. Shadangi, S. Rakshit, J. F. Kennedy, V. K. Gupta and M. Sharma, *Renewable Sustainable Energy Rev.*, 2023, **187**, 113700.

202 M.-Y. Chen, Y.-B. Huang, H. Pang, X.-X. Liu and Y. Fu, *Green Chem.*, 2015, **17**, 1710–1717.

203 H. Kim, S. Yang, Y. H. Lim, J.-M. Ha and D. H. Kim, *J. Hazard. Mater.*, 2022, **423**, 126525.

204 I. Yati, A. A. Dwiatmoko, J. S. Yoon, J.-W. Choi, D. J. Suh, J. Jae and J.-M. Ha, *Appl. Catal., A*, 2016, **524**, 243–250.

205 H. Zhang, T. Yang, Y. Tong, B. Li, J. Wang and R. Li, *Fuel*, 2024, **368**, 131620.

206 H. Guo, J. Zhao, Y. Chen, X. Lu, Y. Yang, C. Ding, L. Wu, L. Tan, J. Long, G. Yang, Y. Tang, N. Tsubaki and X. Gu, *ACS Catal.*, 2024, **14**, 703–717.

207 Y. Xu, Z. Liu, B. Liu, B. Dong, Y. Pan, Y. Li, Y. Li, H. Guo, Y. Chai and C. Liu, *Mol. Catal.*, 2024, **553**, 113761.

208 Y.-H. Kang, J. Gao, X.-Q. Zhang, Y. Gao, Z.-H. Wang, Y.-J. Li, G.-H. Liu, X.-R. Ma, A.-M. Wang, J.-J. Bai, Z.-M. Zong and X.-Y. Wei, *Ind. Crops Prod.*, 2023, **198**, 116704.

209 H. Ali, T. Vandevyvere, J. Lauwaert, S. K. Kansal, M. K. Sabbe, S. Saravanamurugan and J. W. Thybaut, *Catal. Sci. Technol.*, 2023, **13**, 1140–1153.

210 X. Gao, R. Ma, Z. Liu, S. Wang, Y. Wu and G. Song, *Appl. Catal., B*, 2024, **352**, 124059.

211 Z. Li, Z. Li, M. Wu, Z. Qiu, Y. Zhu and R. Zhang, *Mol. Catal.*, 2024, **557**, 113987.

212 Y. Wang, H. Wang, J. Han, Q. Ge and X. Zhu, *Chem. Eng. Res. Des.*, 2023, **199**, 49–60.

213 M. Saidi and P. Moradi, *Chem. Eng. Process.*, 2023, **191**, 109447.

214 S. Wang, D. Xu, Y. Chen, S. Zhou, D. Zhu, X. Wen, Y. Yang and Y. Li, *Catal. Sci. Technol.*, 2020, **10**, 3015–3023.

215 S. Gundekari and S. K. Karmee, *ChemistrySelect*, 2021, **6**, 1715–1733.

216 S. Chen, W. Wang, X. Li, P. Yan, W. Han, T. Sheng, T. Deng, W. Zhu and H. Wang, *J. Energy Chem.*, 2022, **66**, 576–586.

217 Y. Zhu, Y. Ma, Y. Sun, L. Wang, J. Ding, Y. Zhong, J. Zhang, L. Wang and Y. Li, *Renewable Energy*, 2023, **217**, 119222.

218 C. Zhang, X. Zhang, J. Wu, L. Zhu and S. Wang, *Appl. Energy*, 2022, **328**, 120199.

219 A. Kumar, A. Kumar, D. M. Santosa, H. Wang, P. Zuo, C. Wang, A. Mittal, R. Gieleciak, D. P. Klein, M. J. Manto and Y. Bin, *Appl. Catal., A*, 2024, **676**, 119649.

220 H. Duan, J. Dong, X. Gu, Y.-K. Peng, W. Chen, T. Issariyakul, W. K. Myers, M.-J. Li, N. Yi, A. F. R. Kilpatrick, Y. Wang, X. Zheng, S. Ji, Q. Wang, J. Feng, D. Chen, Y. Li, J.-C. Buffet, H. Liu, S. C. E. Tsang and D. O'Hare, *Nat. Commun.*, 2017, **8**, 591.

221 T. Li, Y. Meng, L. Yin, B. Sun, W. Zhu, J. Su and K. Wang, *Appl. Catal., B*, 2024, **353**, 124092.

222 H. Jiao, G. Xu, Y. Sang, H. Chen and Y. Li, *Catal. Today*, 2024, **430**, 114542.

223 F.-P. Wu, L.-L. Qiu, Y.-P. Zhao, Z.-P. Fu, J. Xiao, J. Li, F.-J. Liu, J. Liang and J.-P. Cao, *Fuel Process. Technol.*, 2023, **252**, 107977.

224 C. A. Teles, C. Ciotonea, A. L. Valant, C. Canaff, J. Dhainaut, J.-M. Clacens, F. B. Noronha, F. Richard and S. Royer, *Appl. Catal., B*, 2023, **338**, 123030.

225 F. Yang, D. Liu, Y. Zhao, H. Wang, J. Han, Q. Ge and X. Zhu, *ACS Catal.*, 2018, **8**, 1672–1682.

226 M. Ye, Y. Li, Z. Yang, C. Yao, W. Sun, X. Zhang, W. Chen, G. Qian, X. Duan, Y. Cao, L. Li, X. Zhou and J. Zhang, *Angew. Chem., Int. Ed.*, 2023, **62**, e202301024.

227 P. M. Mortensen, J.-D. Grunwaldt, P. A. Jensen and A. D. Jensen, *Catal. Today*, 2016, **259**, 277–284.

228 C. Ju, M. Li, Y. Fang and T. Tan, *Green Chem.*, 2018, **20**, 4492–4499.

229 P. He, Q. Yi, H. Geng, Y. Shao, M. Liu, Z. Wu, W. Luo, Y. Liu and V. Valtchev, *ACS Catal.*, 2022, **12**, 14717–14726.

230 W. Luo, W. Cao, P. C. A. Bruijnincx, L. Lin, A. Wang and T. Zhang, *Green Chem.*, 2019, **21**, 3744–3768.

231 Y. Zhang, G. Fan, L. Yang, L. Zheng and F. Li, *ACS Sustainable Chem. Eng.*, 2021, **9**, 11604–11615.

232 X. Jia, W. An, Z. Wang and J. Zhou, *J. Phys. Chem. C*, 2019, **123**, 16873–16882.

233 M. Sun, Y. Zhang, W. Liu, X. Zhao, H. Luo, G. Miao, Z. Wang, S. Li and L. Kong, *Green Chem.*, 2022, **24**, 9489–9495.

234 C. Lin, Y. Deng, Y. Lin, J. Li, J. Tu and R. Shu, *Ind. Eng. Chem. Res.*, 2025, **64**, 8170–8178.

235 P.-J. Hsu, J.-W. Jiang and Y.-C. Lin, *ACS Sustainable Chem. Eng.*, 2018, **6**, 660–667.

236 P. Yan, X. Tian, E. M. Kennedy, O. P. Tkachenko and M. Stockenhuber, *ACS Sustainable Chem. Eng.*, 2021, **9**, 15673–15682.

237 Z. Xiang, W. Wang, F. Zhou, H. Zhang, Y. Wang, W. Zhu and H. Wang, *Fuel Process. Technol.*, 2024, **256**, 108073.

238 A. J. R. Hensley, Y. Wang and J.-S. McEwen, *Surf. Sci.*, 2014, **630**, 244–253.

239 Y. Geng and H. Li, *ChemSusChem*, 2022, **15**, e202102495.

240 W. Wang, S. Li, Q. Qiang, K. Wu, X. Pan, W. Su, J. Cai, Z. Shen, Y. Yang, C. Li and T. Zhang, *Angew. Chem., Int. Ed.*, 2024, **63**, e202404683.

241 H. Kim, J. H. Park, J.-M. Ha and D. H. Kim, *ACS Catal.*, 2023, **13**, 11857–11870.

242 Q. Han, M. U. Rehman, J. Wang, A. Rykov, O. Y. Gutiérrez, Y. Zhao, S. Wang, X. Ma and J. A. Lercher, *Appl. Catal., B*, 2019, **253**, 348–358.

243 S. Gao, D. Yu, S. Zhou, C. Zhang, L. Wang, X. Fan, X. Yu and Z. Zhao, *J. Mater. Chem. A*, 2023, **11**, 19210–19243.

244 T. Prasomsri, T. Nimmanwudipong and Y. Román-Leshkov, *Energy Environ. Sci.*, 2013, **6**, 1732–1738.

245 X. Zhang, J. Wu, T. Li, C. Zhang, L. Zhu and S. Wang, *Chem. Eng. J.*, 2022, **429**, 132181.

246 S. Jiang, N. Ji, X. Diao, H. Li, Y. Rong, Y. Lei and Z. Yu, *ChemSusChem*, 2021, **14**, 4377–4396.

247 C. Wang, L. Guo, K. Wu, X. Li, Y. Huang, Z. Shen, H. Yang, Y. Yang, W. Wang and C. Li, *J. Energy Chem.*, 2023, **84**, 122–130.

248 M. J. Hidajat, A. Riaz and J. Kim, *Chem. Eng. J.*, 2018, **348**, 799–810.

249 Z. Zheng, Z. Luo and C. Zhao, *ChemCatChem*, 2018, **10**, 1376–1384.

250 Y. Xin, Z. Zheng, Z. Luo, C. Jiang, S. Gao, Z. Wang and C. Zhao, *Green Energy Environ.*, 2022, **7**, 1014–1023.

251 J. Zhang, J. Sun and Y. Wang, *Green Chem.*, 2020, **22**, 1072–1098.

252 L. Li, L. Dong, X. Liu, Y. Guo and Y. Wang, *Appl. Catal., B*, 2020, **260**, 118143.

253 X. Wang, S. Feng, Y. Wang, Y. Zhao, S. Huang, S. Wang and X. Ma, *Green Energy Environ.*, 2023, **8**, 927–937.

254 M. Zhang, Y. Wu, X. Han, Y. Zeng and C. C. Xu, *Chem. Eng. J.*, 2022, **446**, 136952.

255 W. Jin, J. Gandara-Loe, L. Pastor-Pérez, J. J. Villora-Picó, A. Sepúlveda-Escribano, R. Rinaldi and T. R. Reina, *Renewable Energy*, 2023, **215**, 118907.

256 Z. Wang, Y. Zeng, W. Lin and W. Song, *Int. J. Hydrogen Energy*, 2017, **42**, 21040–21047.

257 T. Yang, L. Shi, R. Li, B. Li and X. Kai, *Fuel Process. Technol.*, 2019, **184**, 65–72.

258 W. Liu, W. You, W. Sun, W. Yang, A. Korde, Y. Gong and Y. Deng, *Nat. Energy*, 2020, **5**, 759–767.

259 H. Shafaghat, P. S. Rezaei and W. M. A. W. Daud, *RSC Adv.*, 2015, **5**, 103999–104042.

260 D. Verma, H.-J. Chun, N. Karanwal, J. Choi, S. Oh, S. M. Kim, S. K. Kim and J. Kim, *Chem. Eng. J.*, 2024, **490**, 151420.

261 B. Sridharan, I. O. Nijeweme, E. Wilbers, G. Gerritsen, J. G. M. Winkelman, R. H. Venderbosch and H. J. Heeres, *J. Anal. Appl. Pyrolysis*, 2024, **183**, 106813.

262 J. Xiao, C. Song, X. Ma and Z. Li, *Ind. Eng. Chem. Res.*, 2012, **51**, 3436–3443.

263 H. Zhao, X. Hu, J. Hao, N. Li, K. Zhi, R. He, Y. Wang, H. Zhou and Q. Liu, *Appl. Catal., A*, 2020, **591**, 117378.

264 S. Jiang, R. Shu, A. Wang, Z. Deng, Y. Xiao, J. Li, Q. Meng and Q. Zhang, *Green Chem.*, 2024, **26**, 9330–9345.

265 Z. Jia, N. Ji, X. Diao, X. Li, Y. Zhao, X. Lu, Q. Liu, C. Liu, G. Chen, L. Ma, S. Wang, C. Song and C. Li, *ACS Catal.*, 2022, **12**, 1338–1356.

266 M. Zhao, J. Hu, P. Lu, S. Wu, C. Liu and Y. Sun, *Fuel*, 2022, **326**, 125020.

267 L. Hu, X.-Y. Wei, M.-L. Xu, Y.-H. Kang, X.-H. Guo, F.-B. Zhang, Z.-M. Zong and H.-C. Bai, *J. Environ. Chem. Eng.*, 2021, **9**, 106599.

268 H. Ruan, Y. Qin, J. Heyne, R. Gieleciak, M. Feng and B. Yang, *Fuel*, 2019, **256**, 115947.

269 J. S. Heyne, A. L. Boehman and S. Kirby, *Energy Fuels*, 2009, **23**, 5879–5885.

270 M. Romanczyk, J. H. R. Velasco, L. Xu, P. Vozka, P. Dissanayake, K. E. Wehde, N. Roe, E. Keating, G. Kilaz, R. W. Trice, D. J. L. Prak and H. Kenttämaa, *Fuel*, 2019, **238**, 483–492.

271 R. C. Boehm, C. Faulhaber, L. Behnke and J. Heyne, *Fuel*, 2024, **371**, 132049.

272 L. E. Caceres-Martinez, J. S. Lopez, R. A. Dagle, R. Gillespie, H. I. Kenttämaa and G. Kilaz, *Fuel*, 2024, **358**, 129986.

273 S. Kosir, R. Stachler, J. Heyne and F. Hauck, *Fuel*, 2020, **281**, 118718.

274 Z. Yang, S. Kosir, R. Stachler, L. Shafer, C. Anderson and J. S. Heyne, *Fuel*, 2021, **292**, 120345.

275 J. Heyne, B. Rauch, P. Le Clercq and M. Colket, *Fuel*, 2021, **290**, 120004.

276 A. Kumar, D. C. Bell, Z. Yang, J. Heyne, D. M. Santosa, H. Wang, P. Zuo, C. Wang, A. Mittal, D. P. Klein, M. J. Manto, X. Chen and B. Yang, *Fuel Process. Technol.*, 2024, **263**, 108129.

277 M. S. Webber, Z. Yang, D. C. Bell, D. G. Brandner, J. R. Bussard, J. Watson, M. L. Stone, X. Wu, Q. S. Neuendorf, L. C. Myers, J. S. Heyne, G. T. Beckham and Y. Román-Leshkov, *Cell Rep. Phys. Sci.*, 2025, **6**, 102687.

278 P. Vozka, D. Vrtiška, P. Šimáček and G. Kilaz, *Energy Fuels*, 2019, **33**, 3275–3289.

279 S. Kosir, J. Heyne and J. Graham, *Fuel*, 2020, **274**, 117832.

280 R. C. Boehm, Z. Yang and J. S. Heyne, *Energy Fuels*, 2022, **36**, 1916–1928.

281 D. J. L. Prak, J. M. Fries, R. T. Gober, P. Vozka, G. Kilaz, T. R. Johnson, S. L. Graft, P. C. Trulove and J. S. Cowart, *J. Chem. Eng. Data*, 2019, **64**, 1725–1745.

282 J. Huo, Z. Wang, P. Lauri, J. D. Medrano-García, G. Guillén-Gosálbez and S. Hellweg, *Environ. Sci. Technol.*, 2024, **58**, 13748–13759.

283 S. S. Wong, R. Shu, J. Zhang, H. Liu and N. Yan, *Chem. Soc. Rev.*, 2020, **49**, 5510–5560.

284 A. W. Bartling, M. L. Stone, R. J. Hanes, A. Bhatt, Y. Zhang, M. J. Biddy, R. Davis, J. S. Kruger, N. E. Thornburg, J. S. Luterbacher, R. Rinaldi, J. S. M. Samec, B. F. Sels, Y. Román-Leshkov and G. T. Beckham, *Energy Environ. Sci.*, 2021, **14**, 4147–4168.

285 A. Kumar, Y. Khani, C. H. Ko, J. Jae, A. Banerjee, T. Bhaskar and Y.-K. Park, *ACS Sustainable Chem. Eng.*, 2024, **12**, 10786–10804.

286 G. Bagnato and A. Sanna, *Catalysts*, 2019, **9**, 1021.

287 Z. Yang, K. Qian, X. Zhang, H. Lei, C. Xin, Y. Zhang, M. Qian and E. Villota, *Energy*, 2018, **154**, 289–297.

288 J. Weyand, S. Adelung, J. Wallinder, B. Sridharan, R. Venderbosch, H. J. Heeres and R.-U. Dietrich, *J. Cleaner Prod.*, 2025, **500**, 144559.

289 K. Witthayolankowit, A. Marson, K. R. Baddigam, D. Lebedeva, M. Shaikh, A. Kane, D. Gupta, M. I. Wide, A. P. Mathew, D. Kubička, A. Manzardo and J. S. M. Samec, *Chem. Eng. J.*, 2023, **470**, 144179.

290 Q. Qian, Z. Luo, Q. Wei, J. Shi, P. Li and E. R. Naranov, *Energy Convers. Manage.*, 2026, **348**, 120630.

291 B. C. Klein, B. Scheidemantle, R. J. Hanes, A. W. Bartling, N. J. Grundl, R. J. Clark, M. J. Biddy, L. Tao, C. T. Trinh, A. M. Guss, C. E. Wyman, A. J. Ragauskas, E. G. Webb, B. H. Davison and C. M. Cai, *Energy Environ. Sci.*, 2024, **17**, 1202–1215.